



## Open Archive Toulouse Archive Ouverte







OATAO is an open access repository that collects the work of Toulouse researchers and makes it freely available over the web where possible

This is an author's version published in: <https://oatao.univ-toulouse.fr/26080>

### Official URL:

<https://doi.org/10.1016/j.msec.2019.110257>

### To cite this version:

Das, Pritam  and Remigy, Jean-Christophe  and Lahitte, Jean-François   
and van der Meer, Andries D. and Garmy-Susini, Barbara and Coetsier, Clémence   
and Desclaux, Sandrine  and Bacchin, Patrice  *Development of double  
porous poly ( $\epsilon$  - caprolactone)/chitosan polymer as tissue engineering scaffold.*  
(2020) *Materials Science and Engineering C*, 107. 110257. ISSN 0928-4931.

Any correspondence concerning this service should be sent  
to the repository administrator: [tech-oatao@listes-diff.inp-toulouse.fr](mailto:tech-oatao@listes-diff.inp-toulouse.fr)

# Development of double porous poly ( $\epsilon$ - caprolactone)/chitosan polymer as tissue engineering scaffold

Pritam Das<sup>a,b,c</sup>, Jean-Christophe Remigy<sup>a</sup>, Jean-François Lahitte<sup>a</sup>, Andries D. van der Meer<sup>b</sup>, Barbara Garmy-Susini<sup>c</sup>, Clémence Coetsier<sup>a</sup>, Sandrine Desclaux<sup>a</sup>, Patrice Bacchin<sup>a,\*</sup>

<sup>a</sup> Laboratoire de Génie Chimique, Université de Toulouse, CNRS UMR, 5503, INPT, UPS, Toulouse, France

<sup>b</sup> University of Twente, Applied Stem Cell Technologies, TechMed Centre, Faculty of Science and Technology, Enschede, 7500, AE, the Netherlands

<sup>c</sup> Institut des maladies métaboliques et cardiovasculaires (I2MC), Université de Toulouse, Inserm U1048, UPS, Toulouse, France

## A B S T R A C T

### Keywords:

Poly ( $\epsilon$  -caprolactone)

Chitosan

Double porous

Membrane

Biocompatibility

Cell culture

Polymer blend made from poly( $\epsilon$  - caprolactone)/chitosan (PCL/CHT) offers interesting opportunities for biological applications. The paper presents a new way to fabricate PCL/CHT double-porosity (macrovoids with interconnected microporosity) membrane materials from a chemical optimization of the solvent and non-solvent phases and from a modified phase inversion technique. By varying the PCL/CHT proportion, it is shown that it is possible to improve the chemical and physical properties of the CHT carbohydrate polymer. The PCL/CHT membranes are fully characterized in term of physico-chemical properties (ATR-FTIR, XRD and DSC) to understand the miscibility of the two-polymer blend. Morphological characterization by SEM shows that by increasing CHT wt% in the blend, the size of the macrovoids was increasing. Rapid enzymatic degradation of PCL from all the blend was found by using lipase (from *P. cepacia*). The mechanisms at the origin of the morphological structuration of the material is also discussed. To test the ability to operate these materials as small diameter vascular scaffolds, cell culture with human umbilical vein endothelial cells (HUVECs) were carried out on the membrane and the results analyzed with laser scanning confocal microscopy (LSCM). Data suggest that the blend membrane with higher concentration of CHT polymer wt% have suitable properties that promote high number of cells on the surface by maintaining cellular cytoskeleton integrity within 3 days. The blend membrane with a double porous morphology could be potentially applicable in future for small diameter vascular graft application. The surface macrovoids (20-90  $\mu\text{m}$ ) could be useful for three-dimensional cellular adhesion and proliferation and interconnected microporous spongy network (7-20  $\mu\text{m}$ ) is expected to transfer essential nutrients, oxygen, growth factor between the macrovoids and the supernatant.

## 1. Introduction

Tissue engineering relies on the use of artificial degradable porous material scaffold integrated with biological cells or molecules to regenerate tissues [1]. The scaffold material should offer specific functionalities to accomplish this goal. Several studies show that 3D structures of the support material control the cell growth [2]. The material composition is a key point that controls the biocompatibility, the cell adhesion and optionally the biodegradability. The material engineering must be tailored to the biological strategy. In recent studies, artificial vascular grafts generally have been fabricated from synthetic polymers, such as polyester, e.g. polycaprolactone (PCL) or polylactic acid (PLA)

or polylactic-co-glycolic acid (PLGA) or polyurethane [3,4]. This kind of polymer scaffolds can provide sufficient mechanical strength and are considered biocompatible and biodegradable without any toxic by-products. However, they are hydrophobic in nature and lack reactive functional sites for further bio-functional modification [5] which led to the development of innovative hybrid materials by mixing both synthetic and natural polymers [6]. Natural carbohydrate polymers like chitosan (CHT) on the other hand can provide an excellent candidate for biomedical vascular grafts application, mostly in combination with other synthetic polymers [7-11]. CHT is a linear polysaccharide composed of glucosamine and N-acetyl glucosamine units connected through  $\beta$ -1,4-glycosidic bond and produced from the highly abundant

*Abbreviations:* PCL, Poly ( $\epsilon$ - caprolactone); CHT, Chitosan; HUVEC, Human umbilical vein endothelial cells; EGM-2, Endothelial growth medium -2; DAPI, 6-Diamidino-2-Phenylindole; BSA, Bovine serum albumin; PBS, Phosphate-buffered saline

\* Corresponding author. Laboratoire de Génie Chimique, Université de Toulouse, CNRS, INPT, UPS, Toulouse, France.

*E-mail address:* [patrice.bacchin@univ-tlse3.fr](mailto:patrice.bacchin@univ-tlse3.fr) (P. Bacchin).

natural polymer, chitin. It is biocompatible, bioresorbable, hydrophilic and non-toxic. It has high affinity towards proteins and provides anti-bacterial, hemostatic, fungistatic, antitumor and anticholesteremic properties [12–16]. It can provide a favorable environment for cell attachment as chemical structure of CHT is similar to glycosaminoglycans (GAGs), which are native components of extracellular matrix (ECM) [17,18]. However, it has low mechanical properties in wet conditions and high hydrophilicity, which can be easily optimized by blending with synthetic polymers. Blending can also improve the low degradation rate of the synthetic polymers in physiological conditions. It is well accepted that blending these two kind of polymers will be very advantageous, which can significantly reduce all the disadvantages and combine the benefits of the individual polymers providing a superior material with good tissue compatibility and sufficient mechanical strength [19–21]. The 3D structure of the material should enable to host the cells but also to distribute the nutrients and to favor the removal of cellular metabolic products.

In the last decades, various scaffolds have been developed more often from an assembly of simple fibers. The study of PCL/CHT blend with electrospinning method is extensively researched and well adaptable for better cell attachment with good dynamic properties [9,10,12,19–25]. However numerous studies report on the difficulties encountered for electrospinning pure chitosan as the structure is mechanically weak, limiting practical processing [26–29]. Furthermore, it is difficult to manage the multiple functionality requirements with an assembly of fibers. The use of membranes appears as an interesting alternative to tune the porosity and to manage the mass transport properties. The different level of membrane porosity can be adjusted in order to have both macrovoids to host the cells and interconnected micropores network to ensure the transportation of molecules [30]. Solvent mixing with PCL and CHT was more conveniently used compared to melt blending which is quite difficult to perform as CHT decomposes before undergoing melting. Although it is also difficult to make a homogeneous blend in solvent mixing due to the high viscosity of CHT in solvent and also the scarcity of good mutual solvents. Several efforts were made as Honma et al. [25,31] produced PCL/CHT blend casting by using common solvent as 1,1,1,3,3,3-hexa-fluoro-2-propanol (HFIP) solution. They showed that PCL/CHT can be processed by using HFIP but this solvent is very expensive, carcinogenic and difficult to remove during washing [32]. Although a different approach was reported to find a good mutual solvent [33–38]. Among them a suitable approach could be to dissolve CHT in 0.5 M acetic acid and PCL in glacial acetic acid where the authors [35] were able to obtain a mixture of these two solutions at a low concentration of polymer but it was not effective at high concentration [31] as in our case. In another study, a solvent mixture of formic acid/acetone was reported to be used to develop PCL/CHT nanofibers at high concentration of polymers. In this case, it was forming beads-like morphology indicating incomplete dissolution of the polymer [39]. Recently, formic acid/acetic acid mixture [40] with certain ratio has produced a mutual solvent for both polymers with minimal degradation and phase segregation but with faster dissolution. Despite so many combination of solvents, the author [40] have reported that the formic acid/acetic acid mixture produced the bead free and least toxic scaffold and the solvent can be easily removed during washing.

Here we propose a new scaffold based on polymer membrane technologies to meet the needs and the constraints discussed above. The main objectives are to obtain a biocompatible and biodegradable material with open macrovoids for three-dimensional cell culture and interconnected microporosities to transport nutrients, oxygen, between the macrovoids and supernatant. The membranes were fabricated from a PCL/CHT blend with a modified liquid induced phase inversion technique in order to create macrovoids on the surface. The percentage ratio of PCL/CHT (100/0, 90/10, 80/20, 70/30 w/w %) blend was changed to investigate a range of chemical interactions, miscibility and biodegradability. The morphology of the developed materials was

observed by SEM and the physico-chemical properties of the blends were characterized by ATR-FTIR mapping, XRD and DSC. In addition, enzymatic degradation study was performed by using lipase (from *Pseudomonas cepacia*; 7U/ml) at 37 °C in phosphate buffer saline (PBS) at physiological pH. Change in morphological properties and weight loss (%) were monitored at predetermined time intervals of the degradation study. To test the biocompatibility and potentialities of the membranes as a small diameter vascular graft for cardiovascular system disease, cell culture was performed with human umbilical vein endothelial cells (HUVECs) up to 3 days and results were observed in laser scanning confocal microscopy.

## 2. Materials and methods

### 2.1. Materials

CHT (MW 190–310 kDa, 75–85% de-acetylation degree, CAS Number 9012-76-4) was purchased from Sigma-Aldrich and PCL (MW 80 kDa, CAPA™ 6800, CAS Number 24980-41-4) was purchased from Perstorp Holding AB, Sweden. Isopore® Polyester (PET) track-etched membranes (with 10 μm pore diameter), used as macrovoid generator, were purchased from Sterlitech, USA. Acetic acid, formic acid, sodium hydroxide and sodium azide (NaN<sub>3</sub>) were purchased from Sigma-Aldrich. Lipase from *Pseudomonas cepacia* (activity: 35U/mg, CAS Number 9001-62-1) were purchased from Sigma-Aldrich. Phosphate buffer saline (PBS) was purchased from Fisher Scientific (CAS Number 7778-77-0). Human umbilical vein endothelial cells (HUVECs) were purchased from Lonza and the corresponding culture medium (EGM-2: basal medium with supplement mix, CC-22011) was obtained from Promocell. Collagen I (rat-tail) were obtained from Santa Cruz. Trypsin-EDTA, Formaldehyde, 6-Diamidino-2-Phenylindole (DAPI), and Alexa Fluor 488 Phalloidin were purchased from Thermo Fisher. Triton X-100, bovine serum albumin (BSA) were purchased from Sigma Aldrich.

### 2.2. Methods

#### 2.2.1. Development of the membrane with a double porosity level

The membranes were developed by modified liquid induced phase inversion method by diffusion between a solvent as formic acid/acetic acid (FA/AA) mixture and non-solvent as NaOH aqueous solution. PCL and CHT with a ratio 100/0, 90/10, 80/20 and 70/30 (w/w%) were dissolved in FA/AA (w/w%) mixture. The polymer concentration in the solution was expressed in wt.% as followed:

$$\text{CHT(wt. \%)} = 100 \frac{\text{Mass}_{\text{CHT}}}{\text{Mass}_{\text{CHT}} + \text{Mass}_{\text{PCL}}} \quad (1)$$

$$\text{Polymer(wt. \%)} = 100 \frac{\text{Mass}_{\text{CHT}} + \text{Mass}_{\text{PCL}}}{\text{Mass}_{\text{CHT}} + \text{Mass}_{\text{PCL}} + \text{Mass}_{\text{Solvents}}} \quad (2)$$

The polymer solution was casted on a glass plate using a casting knife in order to achieve a thickness around 250 μm at 23 °C. The track-etched membrane was at first immersed in the solvent mixture to fill the pores with solvent mixture, slowly wiped out to remove excess solvent and slowly applied on the casted polymer solution (Fig. 1).

The glass plate was then gently immersed in a non-solvent bath containing NaOH solution at 23 °C. Immediately after the immersion, demixing via neutralization of the acidic casted solution was started due to solvent exchange leading to the flat sheet membrane formation in few minutes (in case of PCL/CHT 100/0) to hours (in case of PCL/CHT 70/30). It should be noted that this quenched phase inversion method leads to a thermodynamically non-equilibrium state of the polymers in the final membrane and two different kinds of porous structures were formed in the same condition Fig. 1.

The solvent exchange rate was spatially quite homogeneous where the polymer solution was not covered by the track-etched membrane leading to single porous structure without enough open pores on the top

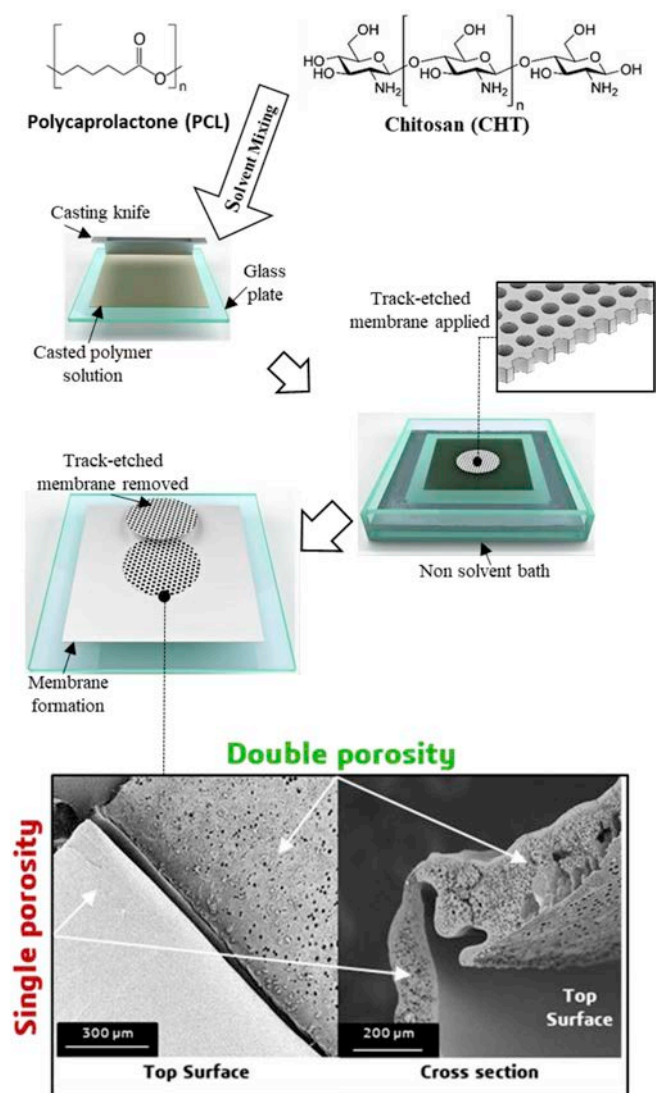


**Fig. 1.** Double porosity development by modified liquid induced phase inversion process with the following steps: PCL/CHT membrane casting, applying the track-etched membrane before immersing in non-solvent bath and removing track-etched membrane after membrane formation. SEM images of PCL/CHT 100/0 represent double porosity and single porosity on top surface and cross section of the same membrane.

surface. On the other hand, where the polymer solution was covered by the track-etched membrane, a heterogeneous solvent exchange was occurred leading to the formation of double porous structure. The macrovoids were formed where the non-solvent has a direct access to the polymer solution through the pores of the track-etched membrane. And, interconnected micropores were formed by diffusion of the non-solvent through the newly formed macrovoids. This mechanism was described by Strathmann et al. [41] to explain the formation of skinned membrane with macrovoids and sponge structure; the nascent skin playing an equivalent role like our track-etched membrane as discussed in Sec. 3.7.

After the membrane formation, when it turned opaque and detached from the glass plate, the track-etched membrane was removed gently. The PCL/CHT membrane was washed several times in ultrapure water and stored in ultrapure water at 4 °C.

The surface where the macrovoids were open towards the non-solvent (i.e. where the track-etched membrane was applied) is denoted as top surface and the other surface, which was facing the glass plate, is denoted as the bottom surface.

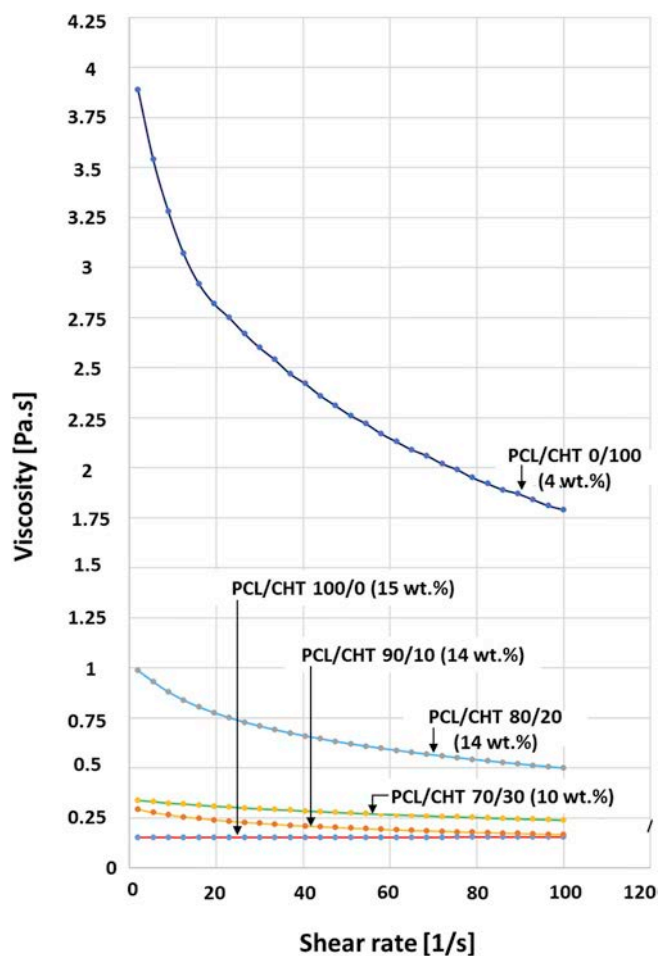


**Fig. 2.** Viscosity [Pa.s] vs shear rate [1/s] measurement of PCL/CHT 100/0 (15 wt%), PCL/CHT 90/10 (14 wt%), PCL/CHT 80/20 (14 wt%), PCL/CHT 70/30 (10 wt%) and PCL/CHT 0/100 (4 wt%) scaffolds respectively in solvent FA/AA mixture.

### 2.2.2. Viscosity measurements of the polymer solution

The viscosity of the polymer solution was measured by Rheometer Anton Paar Physica MCR 301, France (Fig. 2). After complete dissolution of the solution, a 0.6 ml volume was injected on a cone plate rheometer (diameter 50 mm). The viscosity was measured at a shear rate from 2 to 100 s<sup>-1</sup> at 20 °C. All the measurements were performed inside a close chamber in order to avoid the solvent evaporation and dissolution of water from air moisture.

### 2.2.3. Scanning electron microscopic (SEM) analysis

SEM analysis (Phenom XL, Fondis Biotech, France) were done on both double and single porous membranes to evaluate all the developed blend morphology from the top surfaces and the cross sections (Fig. 3).

All the samples were coated with gold and analysis were performed at an accelerating voltage of 10 kV. The surface porosity was also determined from the SEM images by using ImageJ [42] software and reported in Table 1.

### 2.2.4. Attenuated total reflection (ATR)-Fourier transformed infrared (FTIR) spectroscopic analysis and mapping

FTIR analysis were done by using a Nexus Nicolet (USA) FTIR Microscope system with an ATR diamond crystal at 45° angle (Fig. 4). Prior to the examination, 1 cm<sup>2</sup> sample was cut and measurements were done on both surfaces (three times) of each sample. Each point was scanned sixteen times with a resolution of 8 cm<sup>-1</sup> and the spectral range was 650–4000 cm<sup>-1</sup>. The ATR correction was applied on all the



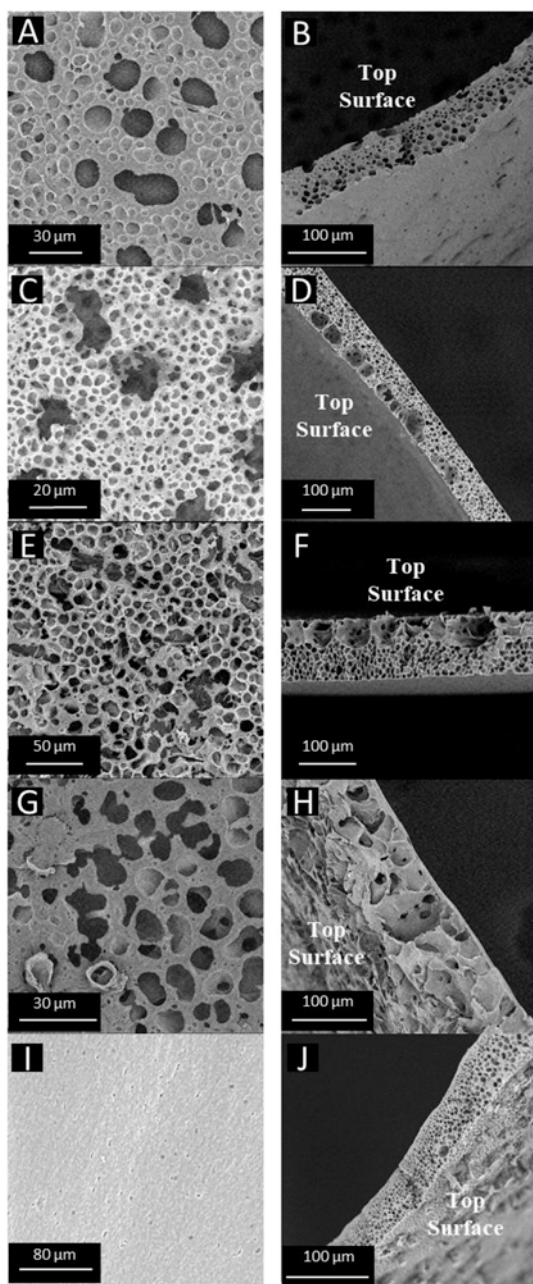


**Fig. 3.** SEM micrographs of membranes on the top surface and cross section with double porosity (using track-etched membrane): (A, B) PCL/CHT 100/0, (C, D) PCL/CHT 90/10, (E, F) PCL/CHT 80/20, (G, H) PCL/CHT 70/30. Single porosity (without using track-etched membrane): (I, J) PCL/CHT 100/0, top surface and cross-section, respectively.

spectra [43]. FTIR chemical mapping on either side of the membrane also performed using an infrared spectrometer IN10MX Thermo-scientific (USA) with an ATR germanium crystal of a 25° angle (Fig. 5). A square sample of 6 mm<sup>2</sup> was studied. Data were analyzed on a 50 μm × 50 μm surface for each point (one point was measured every 50 μm) with a spectral resolution of 8 cm<sup>-1</sup>. Each measurement was scanned by sixteen times with the spectral range 650–4000 cm<sup>-1</sup>.

#### 2.2.5. X-ray diffraction (XRD) analysis

The crystalline structure of membrane sample (5 mm × 5 mm) was investigated by XRD analysis using a D4 Endeavor X-ray diffractometer (CuKα<sub>1</sub> = 0.154056 nm and CuKα<sub>2</sub> = 0.154044 nm; generator 40 eV; 40 mA, Bruker AXS, Karlsruhe, Germany) from 10° to 100° at a scan

**Table 1**

Summary of the polymer blend membrane properties with distinct concentration in correlation with viscosity and pore diameter, melting point.

|                                                                                | PCL/CHT percentage Ratio |        |        |        |       |
|--------------------------------------------------------------------------------|--------------------------|--------|--------|--------|-------|
|                                                                                | 100/0                    | 90/10  | 80/20  | 70/30  | 0/100 |
| Total Polymer Conc. (w/w%)                                                     | 15                       | 14     | 14     | 10     | 4     |
| Solvents HCOOH/AcOH (w/w%)                                                     | 70/30                    | 60/40  | 60/40  | 50/50  | 50/50 |
| Nonsolvent NaOH (M)                                                            | 0.3                      | 0.5    | 0.5    | 0.5    | –     |
| Macrovoid diameter (μm) <sup>a</sup>                                           | 20 ± 3                   | 56 ± 5 | 67 ± 5 | 90 ± 5 | –     |
| Micropore diameter (μm) <sup>a</sup>                                           | 7 ± 3                    | 7 ± 3  | 7 ± 3  | 20 ± 5 | –     |
| Surface Porosity (%) <sup>a</sup>                                              | 40 ± 5                   | 50 ± 5 | 53 ± 5 | 45 ± 5 | –     |
| Viscosity of polymer sol. (Pa.s) @ shear rate 2 sec <sup>-1</sup> <sup>b</sup> | 0.153                    | 0.293  | 0.987  | 0.338  | 3.89  |
| M.P. of PCL in the Blend (T <sub>m</sub> ) °C <sup>c</sup>                     | 61.59                    | 62.78  | 63.19  | 61.70  | –     |

<sup>a</sup> Data were obtained by ImageJ software.

<sup>b</sup> From Fig. 2.

<sup>c</sup> From Fig. 6B.

speed of 21.7 s/step that is equal to 0.02° (2-theta) as can be seen in Fig. 6(A).

#### 2.2.6. Differential scanning calorimetric (DSC) measurements

DSC experiments were conducted (DSC TA instrument Q2000, France) in order to evaluate thermal properties of the PCL/CHT blend membranes (Fig. 6(B)). The membranes were dried at 37 °C and were cut in a dimension of 3 mm<sup>2</sup>. The sample was put inside an aluminum pan and mechanically covered by an aluminum cap. The pre-weighted aluminum pan was placed inside the DSC machine and equilibrate at 20 °C. The temperature scanning was performed at a constant heating rate of 10 °C min<sup>-1</sup>, from 20° to 80 °C without preheating step. The melting point (T<sub>m</sub>) of PCL in the blend by varying CHT wt.% (pure PCL melting point is 60 °C) determined.

#### 2.2.7. Enzymatic degradation of the blend

The membranes were dried in vacuum at 37 °C until constant weight was reached and were cut in 6 mm × 6 mm pieces. The initial weight (w<sub>i</sub>) was taken (in mg up to the fifth decimal point). Then the samples were placed in a 5 ml vials containing 3 ml of PBS 1 × solution, 0.6 mg (7U/ml) of lipase (from *Pseudomonas cepacia*) and 0.05 wt% NaN<sub>3</sub>. The entire procedure was done in a sterile condition and vials were sealed and stored in incubator at 37 °C. The enzyme solution was changed every day in order to maintain the same enzymatic activity during the whole process. The same procedure was done without the enzyme as a control. Three consecutive samples were taken out after 6 h of incubation and every one-day intervals until 10 days. The samples were washed with copious deionized water, dried at 37 °C in vacuum until constant weight. The final weight, W<sub>f</sub>, was taken.

The weight loss, W<sub>loss</sub>%, was calculated by the following equation and can be seen in Fig. 8 (A) and (C) :

$$W_{\text{loss}}\% = 100 \frac{W_i - W_f}{W_i} \quad (3)$$

where, W<sub>i</sub>, is the initial weight and, W<sub>f</sub>, the final weight.

Scanning electron microscopic images of the degraded membranes (Fig. 9) were taken and the ageing solution was collected to observe the change in pH (Fig. 8(B)).

#### 2.2.8. Cell culture and study by laser scanning confocal microscopy

Membranes were cut with diameter of 2.2 cm and washed with sterile phosphate-buffered saline (PBS) three times. The samples were put in 12 well plate and kept in sterile PBS suspension at 4 °C for overnight before the cell seeding. Then the samples were washed again with sterile PBS, 1 ml collagen I (0.1 mg/ml in PBS) was added in the well plate and incubated for 30 min at 37 °C. Then the well plate was taken out from the incubator, washed with PBS and incubated for 1 h

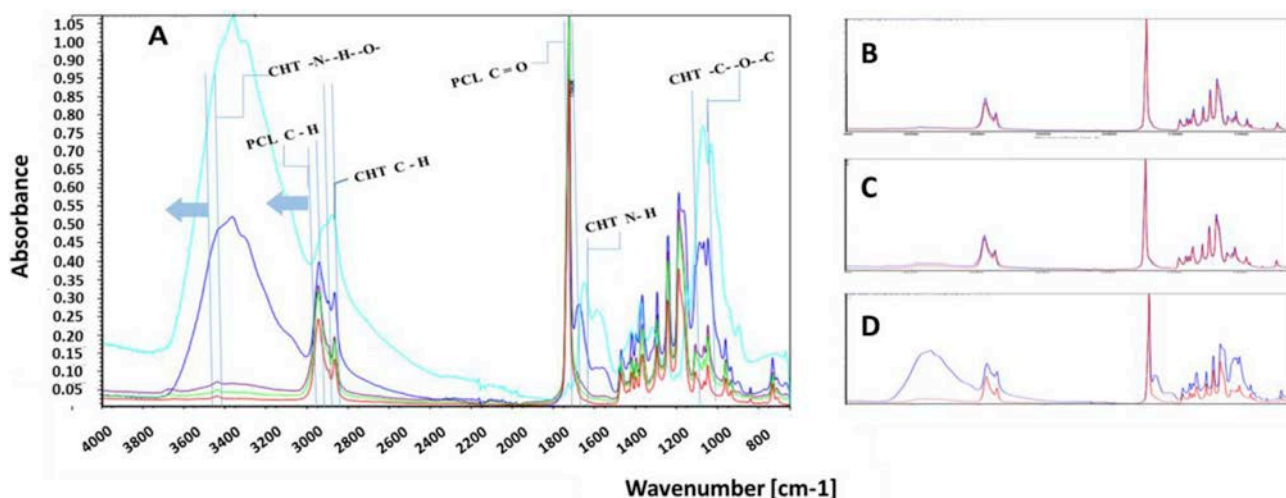


Fig. 4. (A) ATR-FTIR spectra of PCL/CHT scaffold on bottom surface where; PCL/CHT 100/0 in red, PCL/CHT 90/10 in green, PCL/CHT 80/20 in purple, PCL/CHT 70/30 in blue and CHT crude in cyan color respectively. (B, C & D) ATR-FTIR spectra of PCL/CHT 90/10, 80/20 & 70/30 scaffold respectively on either side of same membrane where; top surface in red and bottom surface in blue color respectively. (For interpretation of the references to color in this figure legend, the reader is referred to the Web version of this article.)

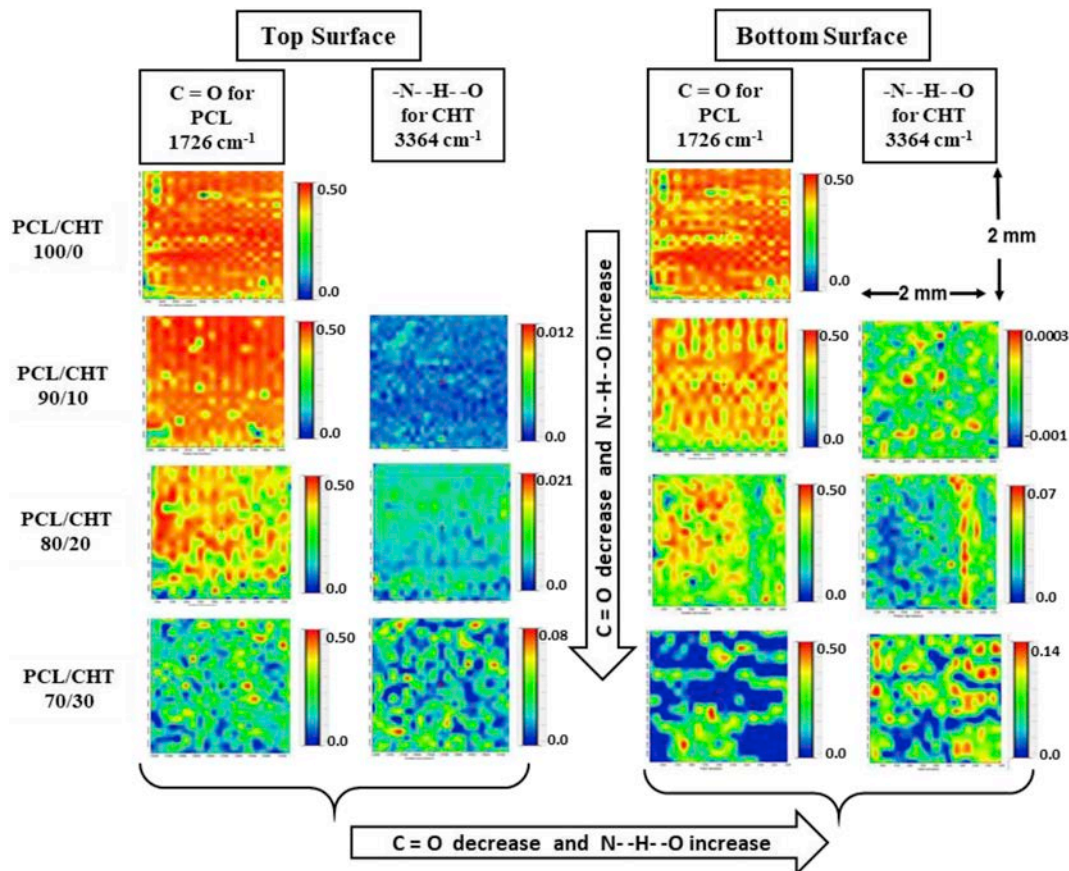


Fig. 5. Chemical mapping of PCL/CHT blends on either surface on the same membrane where; C=O for PCL observed at  $1726\text{ cm}^{-1}$  and hydrogen bonded N-H and O-H observed at  $3364\text{ cm}^{-1}$ . Red and blue colors indicate the intensity of the corresponding bands, high and low intensity, respectively, corresponding to high and low concentration. (For interpretation of the references to color in this figure legend, the reader is referred to the Web version of this article.)

with EGM-2 culture medium (Lonza). Meanwhile, human umbilical vein endothelial cells (HUVECs from Lonza) were trypsinized (passage 4) and collected from a confluent T175 flask. The well plate was taken inside a sterile hood and the incubated culture medium was discarded. Then, 3 ml of homogeneous cell suspension ( $4 \times 10^6$  cells/ml or  $10^6$  cells/cm<sup>2</sup>) was pipetted in each well plate and incubated at  $37^\circ\text{C}$  for 2 h to ensure complete attachments. The well plate was taken out of

the incubator, replaced with fresh culture medium to remove non-attached cells and incubated again.

After 3 days, the well plates were taken in sterile hood and prepared for cell staining. At first the well plates were washed with PBS and the cells were fixed by adding 4% formaldehyde for 15 min. Then the wells were washed with PBS and kept in a permeabilization buffer (PB; 9:1 v:v ratio of 11 mg/ml BSA with 1% Triton X-100 in PBS) at room

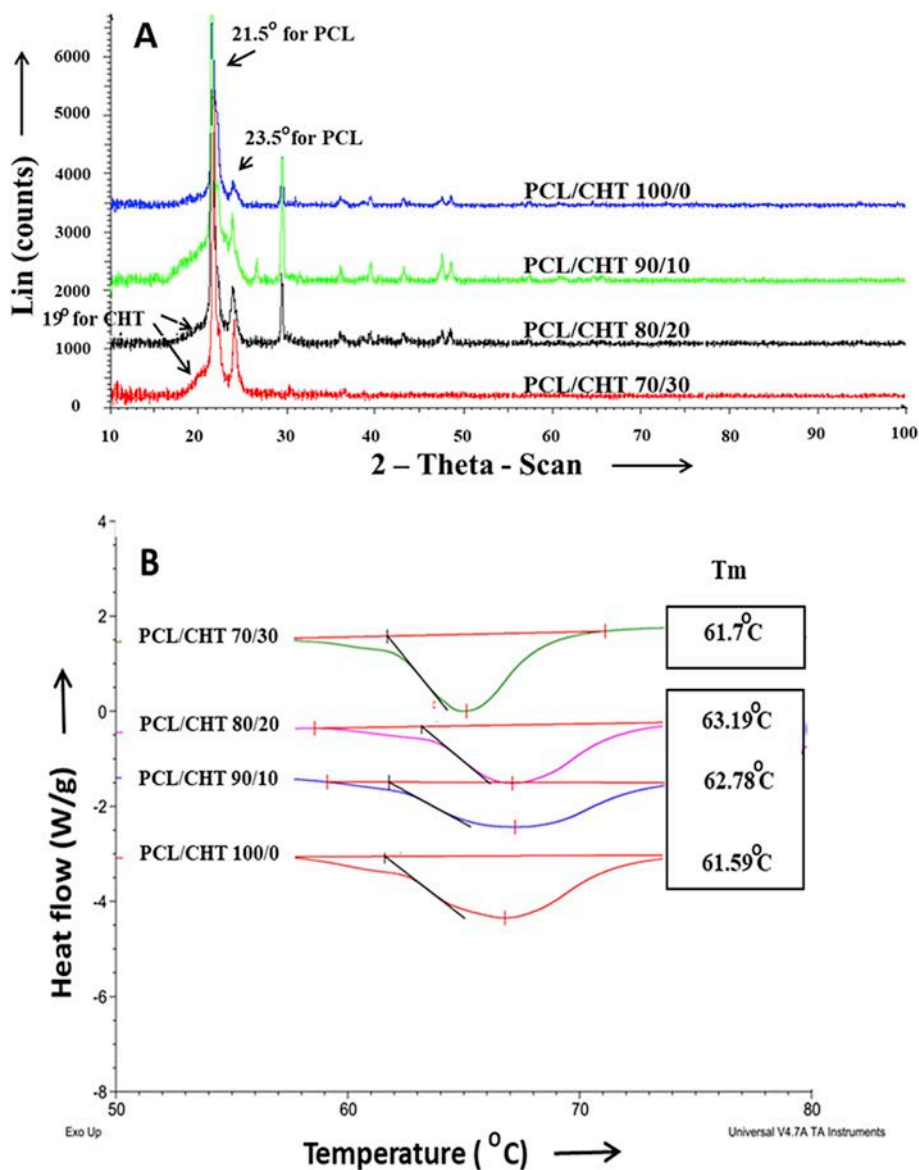


Fig. 6. (A). X-ray diffraction spectra for the different blends, (B) Differential scanning calorimetric study of blends as a function of PCL content in the blend.

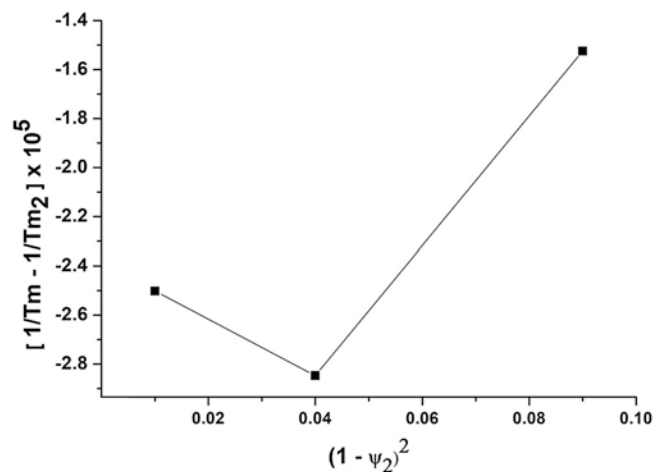


Fig. 7. Nishi – Wang plot. Where  $T_m$  and  $T_{m_2}$  are the equilibrium melting temperature (K) of the blend and pure PCL, respectively, and  $\psi_2$  is the volume fraction of PCL in the blend.

temperature for 15 min to block any non-specific protein-binding sites. Phalloidin-488 and DAPI (Actin Green 488, NucBlue, Thermo Fisher Scientific) were added together in the concentration of 1 drop/ml and 1:4000 in PB, respectively, and incubated at room temperature for 1 h. To prevent photo-bleaching, the well plates were protected from light exposure from this step onwards. Then the well plates were washed thoroughly with PBS and imaged with confocal microscopy (Zeiss LSM 510, Nikon) in  $20\times$  and  $60\times$  magnification (Fig. 12.). As supplementary information, other biological characterizations have been performed with human mesenchymal stem cells (MSCs) in a successive z-stack confocal analysis on these 3D scaffolds [44] and the hydraulic permeability of HUVECs layers have been measured in a microfluidic organ-on-chip device [44,45].

### 3. Results and discussion

#### 3.1. Polymer-solvent-non solvent optimization

Chitosan (CHT) and polycaprolactone (PCL) are polymers with very different chemical properties and finding a common solvent to develop a membrane was an important challenge. Moreover, maintaining an



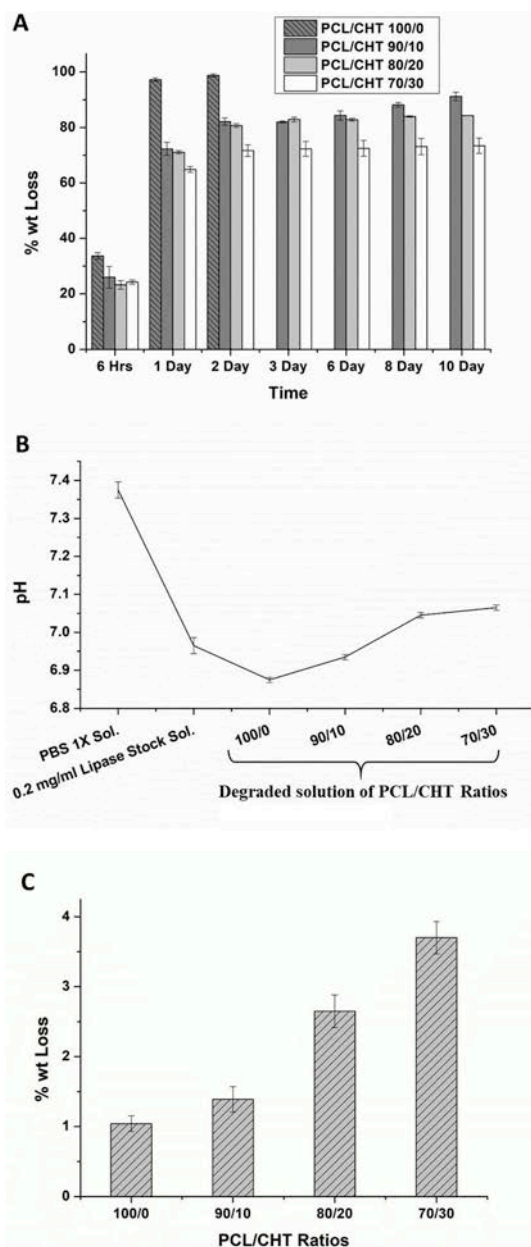


**Fig. 8.** (A) Weight loss % of the sample with lipase enzyme (*Pseudomonas cepacia*; 7 U/ml) at different time intervals, (B) pH of the enzyme degraded solution after the study and (C) weight loss % of the sample without enzyme after 90 days.

optimum viscosity was very important to achieve the double porous membrane structure. The solvent optimization have been partially based on viscosity measurement of the polymer casted solution (Fig. 2) as it was an important parameter that directed the size of the macrovoids during solvent exchange. During solvent mixing, a visible reduction of the viscosity has been observed by dissolving PCL in the common solvent after 2–3 h at temperature more than 35 °C, probably due to the hydrolysis of ester bonds of PCL. In order to avoid the reduction of viscosity, different factors were tuned. CHT was dissolved in the solvent mixture at first at 55 °C for 12 h and then PCL was added when the temperature was below 35 °C. In the common solvent, formic acid was found more responsible for the breakage of PCL ester bonds, although higher wt% of formic acid was better for faster and bead free dissolution. For these reasons, the solvent was also optimized for each PCL/CHT polymer blend according the following composition: PCL/CHT 100/0 (15 wt%) in FA/AA 70/30 (w/w) %, PCL/CHT 90/10 and

80/20 (14 wt%) in FA/AA 60/40 (w/w) % and PCL/CHT 70/30 (10 wt%) in FA/AA 50/50 (w/w) % (Table 1). In these conditions of composition and temperature, a clear, light yellow and viscous solution was obtained within 2 h. After this dissolution step, the polymer solution was kept in stand for 10–20 min before starting the membrane casting. Due to high viscosity of CHT in the solvent mixture, PCL/CHT blend beyond 70/30 ratio was not successful as it was difficult to make a homogeneous mixture of polymer solution by mechanical stirrer and to avoid phase segregation between the two polymers. Viscosity of CHT was remarkably high in the solvent mixture (Fig. 2) that dissolving pure CHT above 4 wt% was difficult and concentration lower than 4 wt% are not sufficient to make a double porous membrane certainly due to lack of good entanglement between the polymer chain or a phase inversion leading to polymer particles.

The viscosity of the final polymer solution of pure PCL, CHT and the different blends were measured and reported in Fig. 2. Results showed that the viscosity of pure CHT of only 4 wt% solution was significantly higher than the viscosity of PCL/CHT 100/0 of 15 wt% solution in the common solvent. This was due to several factors. First of all, the molecular weight of CHT (190 kDa–310 kDa) was higher than the molecular weight of PCL (80 kDa). Secondly, CHT has higher affinity towards the solvent due to the presence of stronger secondary interaction between the functional groups of CHT and the common solvent. As a result, CHT polymer chains likely to be deployed in the solvent leading to higher viscosity [46]. On contrary, in acidic solvent, the viscosity of PCL could be decreased to some extent due to a decrease of the polymer chain length via breakdown of ester linkages. All these effects are responsible for the high difference of solution viscosity between these two polymers.

Concerning the non-solvent, concentration of NaOH more than 0.5 M in the non-solvent bath was responsible to make the membrane fragile by breaking the ester bonds in PCL during membrane formation. Concentration lower than 0.2 M was not sufficiently concentrated to allow the formation of macrovoids. We also varied the concentration of the NaOH solution depending upon the viscosity of the casted solution in order to get consistent macrovoids height of about 50–70% of the total membrane thickness. Finally, a 0.3 M NaOH solution was used for PCL/CHT 100/0 (15 wt%) and 0.5 M NaOH solution was used for the rest of the PCL/CHT blend.

### 3.2. Morphology of the double porous membrane

After the membrane fabrication, the top surface and the cross section morphological characteristics were observed in SEM (Fig. 3). All the scaffolds, which were produced by using the track-etched membrane, are showing double porosity where the macrovoids are open towards the top surface and connected with the spongy microporous network. From the cross section view, it was observed that the localized arrival of the non-solvent inside the polymer solution were creating the macrovoids which were increasing by increasing CHT wt.%. The macrovoids diameter were around  $20 \pm 3$ – $90 \pm 5 \mu\text{m}$  and the diameter of interconnected micropores were around  $7 \pm 3 \mu\text{m}$  (except the PCL/CHT 70/30 ratio for which the micropore diameter was  $20 \pm 5 \mu\text{m}$  (Table 1)).

### 3.3. Chemical characterization by ATR-FTIR spectra

The representative FTIR spectra of the bottom surface of the membrane are shown in Fig. 4 (A). All the stretching and bending vibrations are found to be well matching with the reported values [31]. In crude CHT, the broad peak at  $3364 \text{ cm}^{-1}$  was found due to stretching vibration of intramolecular hydrogen bonding between N–H and O–H. The peak at  $2880 \text{ cm}^{-1}$  was due to the asymmetric bending of C–H group. The N–H and C–O–C peaks were observed at  $1651 \text{ cm}^{-1}$  and  $1070 \text{ cm}^{-1}$  respectively. In PCL, the peaks at  $2946 \text{ cm}^{-1}$  and  $1726 \text{ cm}^{-1}$  represent the characteristic peaks for C–H and ester



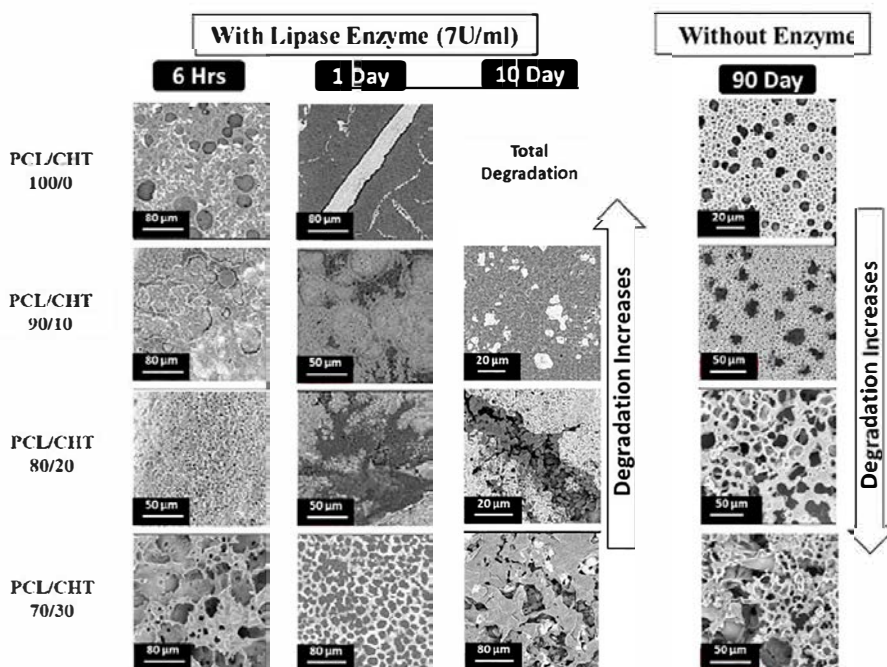


Fig. 9. SEM images of degraded PCL/CHT blends after 6 h, 1 day and 10 days with lipase enzyme (*Pseudomonas cepacia*; 7 U/ml) and after 90 days without enzyme.

carbonyl (C=O) groups respectively. In PCL/CHT blend, by decreasing CHT proportion, the stretching vibration of intramolecular hydrogen bonding between N-H and O-H, shifted towards higher wavenumber region from  $3364\text{ cm}^{-1}$  in PCL/CHT 70/30 to  $3437\text{ cm}^{-1}$  in PCL/CHT 90/10. In addition, the C-H stretching of PCL shifted also towards higher wavenumber region from  $2943\text{ cm}^{-1}$  in PCL/CHT 70/30 to  $2946\text{ cm}^{-1}$  in PCL/CHT 90/10. From all these results, no additional peak was observed indicating presence of no covalent bonding between the two polymers occurred. However, it is clear that the characteristic peak of the blend membrane were constantly shifting by changing the composition likely due to the secondary interaction between the functional groups of two polymers [20,47]. These interactions indicate no phase separation occurs between CHT and PCL in accordance with Sarasam et al. [34] and She et al. [38] who observed a negative Flory Huggins parameter for these two polymers.

The penetration depth of ATR-FTIR absorption,  $d_p$ , for a sample is given by the following equation [31]:

$$d_p = \frac{\lambda}{2\pi \sqrt{\sin^2\theta - n_{21}}} \quad (4)$$

where,  $\lambda$ , and  $\theta$  are the wavelength and incident angle ( $30^\circ$ ) respectively.  $n_{21}$  is the ratio of refractive index of the sample to that of prism. The refractive indices of germanium and polymeric materials are 4.0 and  $\approx 1.5$ , [31], respectively. By putting the wavenumbers corresponding to the characteristic absorption, we obtain a penetration depth around  $\approx 3\mu\text{m}$ , which means that the ATR-FTIR spectra could only gather the information from first few micrometer depth of the surface, whereas the thickness of the membrane sample were around  $80\mu\text{m}$ .

The comparison of ATR-FTIR spectra for either side of the same blend membrane is presented in Fig. 4(B and C, D). One can note that the intensities of specific bands of PCL and CHT are almost the same on the both surface of PCL/CHT 90/10 and PCL/CHT 80/20 membrane indicating almost homogeneous blend. Whereas, in the case of PCL/CHT 70/30, the CHT characteristic peak were higher on the bottom surface indicating probable phase segregation of PCL and CHT through the membrane thickness. From this ATR-FTIR study, one can conclude no phase separation occurs due to the interaction between PCL and CHT but a segregation could occur through the membrane thickness from the

composition of PCL/CHT 70/30 due to distinguished chemical properties of the polymer mentioned earlier.

ATR-FTIR chemical mapping (Fig. 5) of two characteristic bands were observed to highlight the difference of the membrane surface chemistry; C=O ( $1726\text{ cm}^{-1}$ ) for PCL and intramolecular hydrogen bonded N-H and O-H ( $3364\text{ cm}^{-1}$ ) for CHT [21].

From the chemical FTIR mapping, on top and bottom surface, we can verify that by increasing the concentration of CHT in the blends, the absorbance of C=O decreases and the absorbance of intramolecular hydrogen bonded N-H and O-H increases [21,48]. In well agreement with the Fig. 4 (B, C, D), when the intensities are correlated on both the surfaces of the blend, it appears that PCL and CHT have almost the same intensities on PCL/CHT 90/0 and 80/20 indicating no macroscopic phase separation. Whereas, for the blend PCL/CHT 70/30, CHT wt% likely to be higher on the bottom surface than the top surface. Moreover, on the bottom surface of PCL/CHT 70/30, the local concentrations of PCL and CHT at the micrometer scale (i.e. each pixel represents a  $50\mu\text{m} \times 50\mu\text{m}$  of analyzed surface) is seemingly not homogenous as CHT zone are complementary of those of PCL indicating a segregation of both polymers [34,38,49].

### 3.4. Crystalline and thermal properties

Crystalline properties of the blend were measured on a  $1\text{ cm}^2$  dried flat sheet membrane and depicted in Fig. 6 (A). As an amorphous polymer, characteristic broad peak of CHT was hardly observed at  $19^\circ$  in PCL/CHT 80/20 and PCL/CHT 70/30. Characteristic intense peaks at  $21.5^\circ$  and  $23.5^\circ$  at Bragg angles 2-theta corresponding to the (1 1 0) and (2 0 0) planes in PCL can be observed. Moreover, by increasing CHT wt. %, a slight increase of Bragg angles of the characteristic peak of PCL was also observed, indicating an interaction with CHT in agreement with the FTIR data [31,50,51]. It could be interesting to correlate this data with Honma et al. [31], where the differences in the inter-planar spacing of (1 1 0) planes with promoting CHT, the b axes of the PCL orthorhombic cell getting more spread out in the cell. Whereas, no difference was found in the spaces of the (2 0 0) planes. From these results, it can be concluded that significant molecular interaction occurs between PCL and CHT during solvent mixing which is quite contradictory when the blend was produced by melt blending as reported

earlier [52]. It was also reported that by increasing the CHT wt%, the intensity of the characteristic peak of PCL should decrease as the conjugation with PCL and CHT chains suppresses the crystallization of PCL [31,53–55]. Unlike the other reported data, in our case, this effect was not observed and we found a considerable increase of intensity of the PCL specific peak in the blend by increasing CHT wt.%.

Apart from the characteristic peaks of PCL and CHT, some other intense peaks were also detected due to the formation of different type of crystals with different D spacing within the crystal lattice [51]. Those gave an overall crystalline behaviour to the blend. Although in case of PCL/CHT 70/30, those peaks were almost disappear due to significant amorphousness induced by CHT.

DSC analysis Fig. 6 (B) were also performed on the same batch of the sample. Generally, higher a polymer material will have crystallinity, higher energy should be required to break the crystal, hence higher will be the temperature of melting ( $T_m$ ). In our case by increasing CHT wt% the temperature of melting ( $T_m$ ) of the blend was increasing whereas in case of PCL/CHT 70/30 it was decreasing. This phenomena can be correlated with the crystallinity of the blend as discussed above [21].

Generally, pure PCL melts at 60 °C, whereas CHT undergoes thermal degradation at around 270 °C prior to melting [21]. It is still difficult to determine the glass transition ( $T_g$ ) of CHT by conventional thermal technique, although some efforts have been done [52,56,57]. Thus, the variation of the melting point of PCL in the blend was monitored by varying the composition of CHT. Unlike other reported data [21,31,32,35], we found that by increasing CHT wt%,  $T_m$  of the blend increased [51] except PCL/CHT 70/30.

The interaction between the two polymers can be analyzed through the Flory-Huggins interaction parameter ( $\chi_{12}$ ) to correlate temperature of melting and volume fraction of PCL. The equation is evaluated from the simplified Nishi-Wang equation [34,58] for high MW crystalline-amorphous polymer system as follows:

$$\frac{1}{T_m} - \frac{1}{T_{m2}^0} = \frac{-R}{\Delta H_{2u}} \frac{V_{2u}}{V_{1u}} \chi_{12} (1 - \psi_2)^2 \quad (5)$$

where, subscripts 1 and 2 correspond to CHT and PCL polymer, respectively.  $T_m^0$  and  $T_{m2}^0$  are the equilibrium melting temperature (K) of the blend and pure PCL (333.15 K) respectively. R is the universal gas constant (1.98 cal/mol K),  $\Delta H_{2u}$  is the heat of fusion per mole of 100% crystalline PCL (3694.67 cal/mol),  $V_{2u}$  (99.65 cm<sup>3</sup>/mol) and  $V_{1u}$  (1546.82 cm<sup>3</sup>/mol) are molar volumes of the repeating unit of polymers and  $\psi_2$  refers to the volume fraction of PCL in the blend.

The Nishi-Wang plot (Fig. 7) shows that our experimental data cannot be represented with a line passing through the origin, indicating that the interaction parameter ( $\chi_{12}$ ) was composition-dependent and cannot be a constant value [34]. From where it could be concluded that like the most cases, in our data, the interaction parameter  $\chi_{12}$  was not playing a decisive role on the melting behaviour of the crystalline-amorphous polymer systems due to elevation of melting point. This was termed as ‘experimental verification’ reported by Nishi et al. [58].

### 3.5. Enzymatic degradation

The enzymatic hydrolysis of polymeric biomaterials is a heterogeneous process that is affected by the mode of interaction between the enzymes and polymer chains. It generally involves four steps: (a) diffusion of the enzyme from the bulk solution to the solid surface, (b) adsorption of the enzyme on the substrate, forming an enzyme–substrate complex, (c) hydrolysis reaction catalyzed by the enzyme, forming smaller, soluble polymeric chain and (d) diffusion of the soluble degradation products from the solid substrate to the solution [29]. The rate of the overall degradation is controlled by the slowest step. The effect of enzymatic degradation by lipase in terms of wt. loss (%) was observed on four batches of samples in Fig. 8 (A). A fast and almost selective degradation of PCL from all the blends within 48 h was found. This was because the concentration of lipase (7 U/ml) in the

experiment was higher than the human physiological condition (0.03–0.190 U/ml) [59–61]. In addition, the enzyme can easily diffuse through the bulk of porous scaffolds as the size of the bulky protein chains of the enzymes (> 10 nm) is more than 100 times smaller than the scaffolds pore size, leading to a faster degradation compared to dense, non-porous scaffolds.

Contrastingly, when the degradation was conducted without enzyme, the degradation of the blend was significantly low (Fig. 8 (C)) [17]. Moreover, Pure PCL showed the lowest degradation and the degradation increases by increasing the CHT wt.%.

The mechanisms leading to the degradation of the PCL and CHT polymers are significantly different. Generally, PCL, like polyester, degrades similarly to lipid hydrolysis, which is highly facilitated by lipase (lipidase) like enzyme. Lipases are water-soluble enzymes that hydrolyze ester bonds of water-soluble substrates such as triglycerides, phospholipids, and cholesteryl esters [62]. Increasing the CHT wt.% (or decreasing PCL wt.%) not only increases the hydrophilicity but also increases the macrovoids size. As a result the porous bulk of scaffolds was more accessible by the enzymatic solution leading to faster degradation via formation of a smaller soluble enzyme–substrate complex [63]. On the other hand, CHT, like polysaccharide, consisting of N-acetyl/deacetyl glucosamine, degrades by oxidative-reductive chain scission and lipase has very weak effect on CHT degradation [64–67]. In case of degradation without enzyme, the ability of the material to swell by absorbing water [68], which was increasing by increasing CHT wt.%, plays a key role for the degradation.

The surface morphology of degraded membrane after different time intervals is presented in the Fig. 9. In case of degradation assay with enzyme, a noticeable damage on the surface of membranes were observed with a significant weight loss.

The change in pH measured in the degraded solution is reported in the Fig. 8 (B). PCL/CHT 100/0 has shown the lowest pH probably due to the presence of higher amount of acidic residue via ester chain degradation. Overall in all the blends, the pH remained very close to the physiological pH (7.4), indicating almost no toxicity of the degraded solution.

### 3.6. Microscopic PCL/CHT chemical structure

The presence of secondary interactions between PCL and CHT was observed above in the FTIR as well as in the crystallinity (with a shift of the characteristic peaks) that allow avoiding phase separation and total immiscibility between the two polymers.

The solvent and non-solvent power can be evaluated through the interaction distances using the Hansen solubility parameter approach [69]. From the Table 2, the interaction distances are found lowest between PCL and the acids (FA/AA), indicating the acids are good solvents for PCL whereas water is a non-solvent with highest interaction distance. On the other hand, the interaction distances between CHT and the acids (FA/AA) was found high (with almost the same non-solvent power), indicating the acids are not good solvent for CHT. However, the solubility of CHT in water at low pH as well as in concentrated acids is usually observed due to strong acid/base interaction, turning CHT to a polyelectrolyte via protonation of amine groups. The use of NaOH solution as a non-solvent is then crucial, as the base will deprotonate the amine groups leading to insoluble CHT. Thus, NaOH solution is a stronger non-solvent of CHT than pure water.

Thus the phase segregation phenomena along the membrane thickness with high CHT wt% (apparently in PCL/CHT 70/30 in our case) can be explained (Fig. 10.) by the presence of a NaOH conc. gradient along the thickness of the polymer solution (i.e. high NaOH conc. at the top to low NaOH conc. at the bottom) during the phase inversion process. The NaOH conc. gradient was created along the thickness of the polymer solution due to faster neutralization at the top surface than at the bottom surface, leading to the formation of conjugate bases (FA<sup>-</sup> and AA<sup>-</sup>, which are non-solvent too). The presence

**Table 2**

Hansen solubility parameter of CHT, PCL and solvents and the interaction distance. All values are given in MPa<sup>1/2</sup>.

|       | $\delta$           | $\delta d$         | $\delta p$         | $\delta h$         | Interaction distance (MPa <sup>1/2</sup> ) |      | Ref.    |
|-------|--------------------|--------------------|--------------------|--------------------|--------------------------------------------|------|---------|
|       | MPa <sup>1/2</sup> | MPa <sup>1/2</sup> | MPa <sup>1/2</sup> | MPa <sup>1/2</sup> | PCL                                        | CHT  |         |
| CHT   | 38,8               | 22,9               | 16,6               | 26,6               | 23,9                                       | –    | [70,71] |
| PCL   | 20,3               | 17,7               | 6,2                | 7,8                | –                                          | 23,9 | [72]    |
| water | 47,8               | 15,5               | 16                 | 42,3               | 36,1                                       | 21,6 | [69]    |
| FA    | 22,6               | 14,6               | 10                 | 14                 | 9,6                                        | 21,9 | [69]    |
| AA    | 21,4               | 14,5               | 8                  | 13,5               | 8,8                                        | 23,0 | [69]    |

of conjugate bases increased the gradient of solvent activity. CHT chains have more affinity for the solvent (FA/AA) than PCL and thus the gradient of chemical potential for CHT is more important than PCL [73]. Due to these differences in chemical potential gradient, CHT should move towards the bottom surface to some extent higher than PCL chains. Whereas PCL chains coagulated on the top surface faster than CHT as water is a strong non solvent of PCL. The PCL chains will be trapped in contact with water and cannot move anymore.

### 3.7. Mesoscopic morphological structuration of the membrane

The equilibrium phase diagram for the ternary system of polymer-solvent-nonsolvent, Fig. 11 (A), can be used to understand the route taken during the membrane precipitation process, leading to the formation of double porosity. Any point within the triangle represents a mixture of three components where the system composed of two phases: a one-phase region, where all components are miscible, and a two-phase region, where the system separates into high viscosity (polymer-rich) and low viscosity (polymer-poor) phases. The liquid-liquid phase boundary is the so-called binodal curve. Every composition inside the binodal curve will demix into two liquid phases which differ in composition but are thermodynamically in equilibrium with each other. The tie line connects a pair of equilibrium compositions in the phase diagram. Thus, at low polymer concentrations where the tie line intersects the binodal, the system is a low viscosity polymer-poor phase. As the concentration of polymer is increased, the viscosity of the system also increases rapidly and the tie line intersects the binodal at high polymer concentration, consider as the gelation point (E), a highly viscous polymer-rich phase that further polymer chain movement is not possible [74,75].

Two extreme cases can be considered according to the PCL/CHT percentage ratio: Case 1 (left column in Fig. 11.) corresponds to the pure PCL blend and case 2 (right column in Fig. 11.) corresponds to the

PCL/CHT blend with lower polymer percentage. As previously discussed, one difference between these cases is the use of higher NaOH solution in the non-solvent phase for higher CHT concentration. In the last case, the gelation point should occur for higher polymer concentration, as there is less attractive interaction between CHT and solvent in basic solution.

Regarding the triangular phase diagram (Fig. 11 (A)), the entire membrane formation process follows the path (A-B-C-D), where A represents the initial casted solution when it is just immersed inside the non-solvent ( $t = 0$ ), B represents the demixing point where the two liquid phases formation start. As the two-phase formation proceed, more solvent was neutralized by increasing the viscosity of the polymer-rich phase. At one point, the viscosity is high enough to restrict further polymer chain movement and the polymer is considered as solid, representing the solidification point C, where it intersects the tie line with the gelation point E. From B to C, the polymer lean phase coalesces to form the observed macrovoid: the extent of the coalescence depends of the time need to go from B to C.

After that, the membrane structure does not evolve and further solvent exchange results in the removal of solvent. Some shrinkage of the bulk volume could also occurs leading to the final membrane structure D [74,76]. The composition D is in equilibrium between the polymer-rich and polymer-poor phase and the position of point D on the polymer/non-solvent line of the phase diagram determines the overall porosity of the membrane.

Due to the presence of the track-etched membrane on the casted solution, just after immersion, the non-solvent has a restricted access to the polymer solution through the pore of the track-etched membrane, initiating a spatially heterogeneous solvent-nonsolvent exchange [30,77]. The phase inversion starts in the zone where there is a direct contact between the polymer and the non-solvent, resulting the initiation and growth of a liquid wall (nascent macrovoids). The liquid wall, created from the phase inversion, expands radially from the non-solvent invasion point (polymer-poor phase) towards the bulk (polymer-rich phase). During the phase inversion, the polymer concentration of the liquid wall increases until the solidification point C and thus further polymer chain movement stops [74,76].

The polymer blend composition, polymer wt.% and non-solvent concentration play an influential role on the macrovoid size and on the membrane porosity. Particularly in the case 2, where CHT is present along with PCL inside the polymer solution, the blend has a higher affinity with solvents than PCL alone. This is due to higher secondary interaction between the CHT functional groups and solvents, higher M.W and the presence of cyclic structure, resulting deployment and high entanglement of CHT chains in the solution [40]. In that case and after the demixing point, the non-solvent first has to disable those

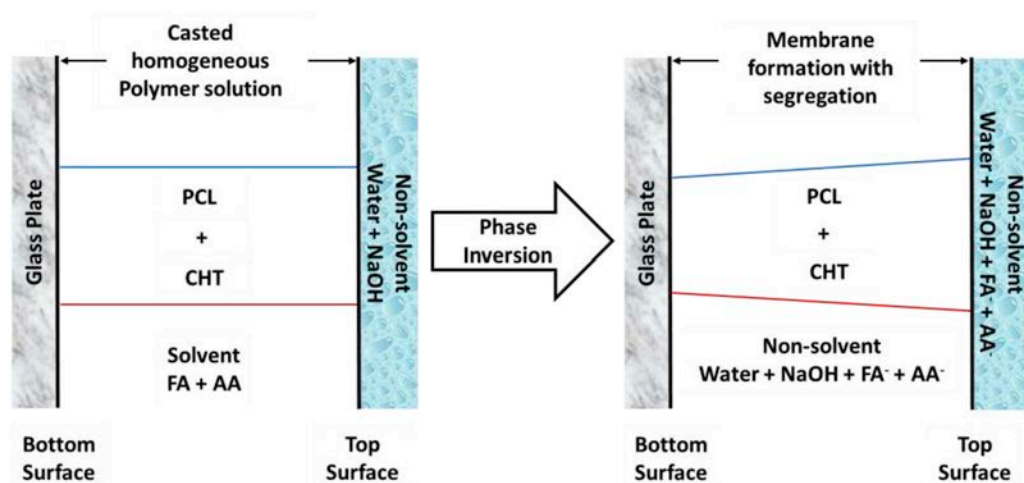
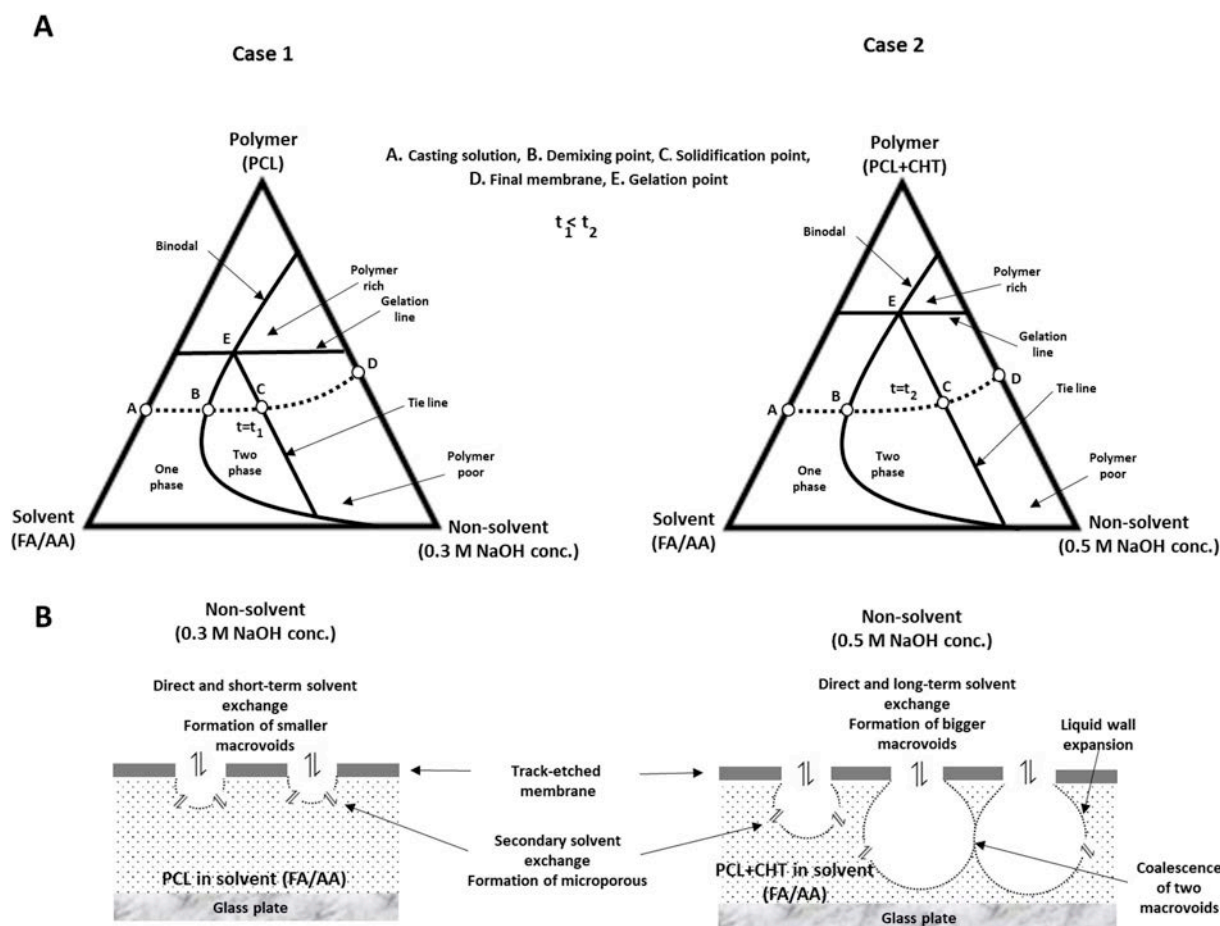


Fig. 10. Qualitative representation of the gradient along the thickness and the differential migration of PCL (in blue) and CHT (in red) in the blend after phase inversion (where PCL is polycaprolactone, CHT is chitosan, FA is formic acid, AA is acetic acid, FA<sup>-</sup> is formate anion and AA<sup>-</sup> acetate anion respectively). (For interpretation of the references to color in this figure legend, the reader is referred to the Web version of this article.)





**Fig. 11.** (A). Schematic phase diagram of the system polymer-solvent-nonsolvent representing the membrane macrovoids formation pathway (A-B-C-D), (B). Illustrative representation of the formation of macrovoids. **Case 1:** formation of smaller macrovoids consisting of polymer as PCL, solvent as FA/AA and non-solvent as NaOH at low concentration and **Case 2:** formation of bigger macrovoids consisting of polymer as PCL + CHT, solvent as FA/AA and non-solvent as NaOH at high concentration (where PCL is polycaprolactone, CHT is chitosan, FA is formic acid, AA is acetic acid respectively).

secondary interaction between CHT and solvents followed by solvent exchange via acid-base reaction, leading to a delay in solidification ( $t = t_2$ , path B-C). Meantime, more non-solvent invades due to a higher non-solvent concentration and lower polymer wt.% (in the case of PCL/CHT 70/30 with 10 wt%). As a result further expansion of the liquid wall takes place and eventually two neighboring nascent liquid walls coalesce before reaching the solidification point C, leading to the formation of larger macrovoids [74,76]. In case 1, due to the presence of PCL alone, after the demixing point, the solvent exchange starts readily as, unlike CHT, PCL does not have strong affinity with the solvents. In addition, due to the lower nonsolvent concentration and higher polymer wt.% (PCL/CHT 100/0 with 15 wt%), the liquid wall reaches the solidification point C ( $t = t_1$ ; where  $t_1 < t_2$ ) before significant expansion, resulting in smaller macrovoids.

A secondary solvent exchange followed by phase inversion also occurs through the whole volume of the polymer solution because of the slow diffusion of the non-solvent through the newly formed macrovoids. The polymer solution area, which is protected from direct exposure from the non-solvent due to the presence of the track-etched membrane, undergoes the secondary solvent exchange. This phase inversion takes place at a slower rate and leads to the formation of a uniform spongy microporous network connected by the macrovoids [30,74,76,77].

Remigy et al. [76] and, earlier, Strathmann et al. [74] reported that, due to the heterogeneous and restricted solvent diffusion, the generation of macrovoid can also be achieved by a dense skin formation on the polymer solution layer via rapid homogeneous precipitation. In that

case, after formation of the dense skin, it disrupts by shrinkage of the homogeneous solid layer and the macrovoid formation starts from the disruption point due to the heterogeneous and restricted access of the non-solvent. In the present work, we cover the polymer solution with track-etched membrane, which acts as a dense skin with restricted access of the non-solvent [30,77]. The use of track-etched membrane and its removal allows the generation of largely open macrovoids, which were not obtained using the classical phase inversion technique. When no track-etched membrane was used, the membrane material presented single porosity like conventional liquid-liquid homogeneous phase inversion and pores were not open enough towards the top surface (Fig. 3. I, J).

### 3.8. Cellular compatibility study by LSCM

The cellular compatibility of the four batch of membranes were observed in confocal images (Fig. 12) at  $20\times$  and  $60\times$  magnification after 3 days of seeding HUVECs. The cell nucleus were stained by DAPI in blue and the actin stress fibers were stained by Phalloidin Alexa Fluor™ 488 in green. The scaffolds were designed to develop as bioactive scaffolds for a tissue engineered vascular grafts to obtain higher endothelial performance by the HUVECs by tuning the physico-chemical and morphological properties of the blends. At  $20\times$  magnification all the membranes are showing a very high number of cells adhered on the membrane. By introducing CHT, all the PCL/CHT blend are showing even higher number of cell-cell and cell-scaffolds interaction than pure PCL membrane and make an almost confluent

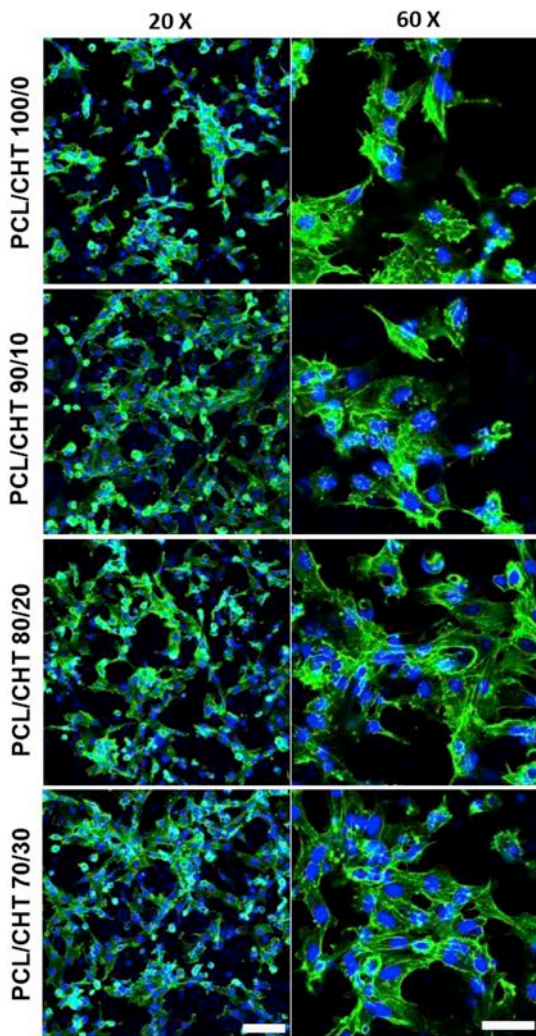


Fig. 12. LSCM images of HUVECs on PCL/CHT membrane after 3 days with staining (nucleus by DAPI in blue and cell cytoskeleton by phalloidin in green). Scale bar: 100  $\mu\text{m}$  in 15  $\times$  mag. and 50  $\mu\text{m}$  60  $\times$  mag. respectively. (For interpretation of the references to color in this figure legend, the reader is referred to the Web version of this article.)

monolayer within 3 days. In 60 $\times$  magnification, we discover that the HUVECs maintain their natural endothelial like morphology by strongly expressing the actin fibers in green, which was significantly visible in PCL/CHT 80/20 and 70/30 blend. These findings clearly suggest that all four batches of scaffolds are highly biocompatible, especially by introducing CHT, likely because of better hydrophilicity, pore spacing and morphology. Du et al. [22] reported rapid HUVECs adhesion and proliferation upon gradient PCL/CHT nanofibrous, electrospun scaffolds than the uniform one due to higher adsorption of VEGF on the CHT rich side (luminal side). Casillo et al. [78] grew endothelial cells on non-porous and porous SiO<sub>2</sub> membranes where they find higher cell-matrix adhesion on the surface with bigger pores probably because the spacing between the pores, and thus the amount of continuous space for the cells to adhere was higher.

The exclusive cellular characterization of these double porous materials was extensively carried out and already reported in previous papers [44,45]. Static cell culture with human mesenchymal stem cells (hMSCs) has been performed for 3 weeks. With confocal images, it was shown that these materials have a good ability to promote cellular invasion and proliferation by increasing CHT wt% [44]. The additional cellular resistance has also been monitored by seeding human umbilical vein endothelial cells (HUVECs) on the membranes embedded inside a

microfluidic organ-on-chip system by mimicking dynamic physiological condition. Here again the results suggest that by increasing CHT wt%, the microstructural and chemical properties were significantly improved resulting in enhanced hydraulic resistance due to increased cellular barrier function [45].

Significant advancement has been made in engineered blood vessels grafts with development of bioscaffolds constructs, providing an alternative to replace the damaged vessel in treating cardiovascular diseases (CVD). The successful implementation of these two kind of cells in our studies could be strategically useful to regenerate small diameter blood vascular system. Human endothelial cells (ECs) can be seeded on the surface of the 3D scaffold (on the luminal side). Whereas seeding the mesenchymal stem cells (MSCs) inside the bulk could be obvious due to two beneficial properties. MSCs could be genetically modified to produce the essential vascular endothelial growth factors (VEGFs) in order to enhance the endothelium [79–81], which is very important, as the damaged endothelium could not produce the VEGFs naturally [82]. MSCs proliferation and viability are highly dependent on environmental cues like material stiffness, growth medium and other physical and mechanical forces [83,84]. With proper environmental condition, MSCs can change their phenotype to smooth muscle cells, which are usually present inside the vessels underneath the endothelium [85–87]. As the cell will grow, the biodegradable scaffold will be gradually replaced by cells and, at the end, the scaffold will be completely absorbed inside the body to achieve the blood vessel construct.

#### 4. Conclusions

A PCL/CHT membrane with a unique double porosity level has been developed for tissue engineering applications. The membrane has been fabricated with a modified phase inversion technique from different ratios of PCL/CHT polymer blends. Macrovoids at the membrane surface have been formed which are connected through membrane microporous network. The physico-chemical properties and morphological structure of the membrane have been characterized and the mechanisms at the origin of the membrane formation have been discussed. This membrane exhibits interesting functionalities for tissue engineering applications:

- The membrane possesses a structure with three dimensional double porosity level, thanks to the micro-patterning techniques. The SEM images show that plenty of micrometers macrovoids (20–90  $\mu\text{m}$ ) are connected through spongy porous network.
- The morphological analysis of the membrane shows that the macrovoids size increased by increasing the Chitosan concentration. ATR-FTIR chemical spectra confirm the presence of secondary interaction between PCL and Chitosan. From the FTIR chemical mapping, we found a slight segregation of polymers along the thickness in case of high Chitosan wt%. From the XRD and DSC studies, we observed an increase of the crystallinity and melting point by increasing CHT wt%.
- The biodegradability of the material can be adjusted according to the PCL/CHT ratio. The enzymatic degradation of the PCL/CHT double porous scaffold using lipase (from *P. cepacia*), pointed out a faster and almost selective degradation of PCL in the blend.
- Human umbilical vein endothelial cells (HUVECs) show rapid adhesion and proliferation on the membranes, especially by introducing chitosan in the blend, by maintaining their natural cellular morphology. PCL/CHT materials allows then to act as a niche to host cells. Such a structure could ensure biofunctionality for tissue repair: where the macrovoids could be useful for three-dimensional cell culture and spongy microporous network could be useful to transport essential nutrients, growth factors and oxygen for cell survival.

The encouraging data obtained in this work demonstrate that these

new double porous PCL/CHT scaffolds have high potential as tissue-engineering scaffolds for artificial vascular grafts application.

#### Declaration of competing interest

None.

#### Acknowledgements

The author wants to acknowledge the funding committee Erasmus Mundus Doctorate in Membrane Engineering (5<sup>th</sup> Ed) – EACEA under European Commission. We like to thank Corinne Routaboul (Service commun de spectroscopie infrarouge et Raman, Université Paul Sabatier, France) for the scanning of samples on the FTIR micro-spectrometer; we thank Christophe Tenailleau (CIRIMAT, Université Paul Sabatier, France) for the x-ray crystallographic analysis.

#### Appendix A. Supplementary data

Supplementary data to this article can be found online at <https://doi.org/10.1016/j.msec.2019.110257>.

#### References

- [1] S.J. Hollister, Porous scaffold design for tissue engineering, *Nat. Mater.* 4 (2005) 518, <https://doi.org/10.1038/nmat1421>.
- [2] M.M. Stevens, J.H. George, Exploring and engineering the cell surface interface, *Science* 310 (2005) 1135–1138, <https://doi.org/10.1126/science.1106587>.
- [3] I. Manavitehrani, A. Fathi, H. Badr, S. Daly, A. Negahi Shirazi, F. Dehghani, Biomedical applications of biodegradable polyesters, *Polymers* 8 (2016) 20, <https://doi.org/10.3390/polym8010020>.
- [4] V.D. Palumbo, A. Bruno, G. Tomasello, G. Damiano, L. Monte, A.I., Bioengineered vascular scaffolds: the state of the art, *Int. J. Artif. Organs* 37 (2014) 503–512, <https://doi.org/10.5301/ijao.5000343>.
- [5] B.P. Tripathi, P. Das, F. Simon, M. Stamm, Ultralow fouling membranes by surface modification with functional polydopamine, *Eur. Polym. J.* 99 (2018) 80–89, <https://doi.org/10.1016/j.eurpolymj.2017.12.006>.
- [6] Yumei Xiao, Dongxiao Li, Xuening Chen, Jian Lu, Hongsong Fan, Xingdong Zhang, Preparation and cytocompatibility of chitosan-modified polylactide, *J. Appl. Polym. Sci.* 110 (2008) 408–412, <https://doi.org/10.1002/app.28493>.
- [7] R.S. Teotia, D. Kalita, A.K. Singh, S.K. Verma, S.S. Kadam, J.R. Bellare, Bifunctional polysulfone-chitosan composite hollow fiber membrane for bioartificial liver, *ACS Biomater. Sci. Eng.* 1 (2015) 372–381, <https://doi.org/10.1021/ab500061j>.
- [8] M. Prabaharan, M.A. Rodriguez-Perez, J.A. de Saja, J.F. Mano, Preparation and characterization of poly(L-lactic acid)-chitosan hybrid scaffolds with drug release capability, *J. Biomed. Mater. Res. B Appl. Biomater.* 81B (2007) 427–434, <https://doi.org/10.1002/jbm.b.30680>.
- [9] F. Chen, X. Li, X. Mo, C. He, H. Wang, Y. Ikada, Electrospun chitosan-P(LLA-CL) nanofibers for biomimetic extracellular matrix, *J. Biomater. Sci. Polym. Ed.* 19 (2008) 677–691, <https://doi.org/10.1163/156856208784089661>.
- [10] A. Di Martino, M. Sittlinger, M.V. Risbud, Chitosan: a versatile biopolymer for orthopaedic tissue-engineering, *Biomaterials* 26 (2005) 5983–5990, <https://doi.org/10.1016/j.biomaterials.2005.03.016>.
- [11] X. Zhou, M. Kong, X.J. Cheng, C. Feng, J. Li, J.J. Li, X.G. Chen, In vitro and in vivo evaluation of chitosan microspheres with different deacetylation degree as potential embolic agent, *Carbohydr. Polym.* 113 (2014) 304–313, <https://doi.org/10.1016/j.carbpol.2014.06.080>.
- [12] S. Hong, G. Kim, Fabrication of electrospun polycaprolactone biocomposites reinforced with chitosan for the proliferation of mesenchymal stem cells, *Carbohydr. Polym.* 83 (2011) 940–946, <https://doi.org/10.1016/j.carbpol.2010.09.002>.
- [13] Q.F. Dang, S.H. Zou, X.G. Chen, C.S. Liu, J.J. Li, X. Zhou, Y. Liu, X.J. Cheng, Characterizations of chitosan-based highly porous hydrogel—the effects of the solvent, *J. Appl. Polym. Sci.* 125 (2012) E88–E98, <https://doi.org/10.1002/app.36681>.
- [14] X. Zhou, X.J. Cheng, W.F. Liu, J. Li, L.H. Ren, Q.F. Dang, C. Feng, X.G. Chen, Optimization and characteristics of preparing chitosan microspheres using response surface methodology, *J. Appl. Polym. Sci.* 127 (2013) 4433–4439, <https://doi.org/10.1002/app.38003>.
- [15] X. Zhou, M. Kong, X. Cheng, J. Li, J. Li, X. Chen, Investigation of acetylated chitosan microspheres as potential chemoembolic agents, *Colloids Surfaces B Biointerfaces* 123 (2014) 387–394, <https://doi.org/10.1016/j.colsurfb.2014.07.044>.
- [16] Q.Q. Wang, M. Kong, Y. An, Y. Liu, J.J. Li, X. Zhou, C. Feng, J. Li, S.Y. Jiang, X.J. Cheng, X.G. Chen, Hydroxybutyl chitosan thermo-sensitive hydrogel: a potential drug delivery system, *J. Mater. Sci.* 48 (2013) 5614–5623, <https://doi.org/10.1007/s10853-013-7356-z>.
- [17] Ana R. Costa-Pinto, Ana M. Martins, Magda J. Castelhana-Carlos, Vitor M. Correlo, Paula C. Sol, Adhemar Longatto-Filho, Mrinal Battacharya, Rui L. Reis, Nuno M. Neves, In vitro degradation and in vivo biocompatibility of chitosan-poly (butylene succinate) fiber mesh scaffolds, *J. Bioact. Compat. Polym.* 29 (2014) 137–151, <https://doi.org/10.1177/088391514521919>.
- [18] W.F. Liu, H.D. Zang, X. Zhou, C.Z. Kang, Y. Li, J. Li, Q.F. Dang, X.J. Cheng, X.G. Chen, The primary culture and subculture of lymphoid cells from shrimp, *Penaeus chinensis* on thermo-sensitive CS/α, β-GP hydrogel, *Aquacult. Res.* 45 (2014) 334–340, <https://doi.org/10.1111/j.1365-2109.2012.03231.x>.
- [19] A. Cooper, N. Bhattarai, M. Zhang, Fabrication and cellular compatibility of aligned chitosan-PCL fibers for nerve tissue regeneration, *Carbohydr. Polym.* 85 (2011) 149–156, <https://doi.org/10.1016/j.carbpol.2011.02.008>.
- [20] V.N. Malheiro, S.G. Caridade, N.M. Alves, J.F. Mano, New poly(ε-caprolactone)/chitosan blend fibers for tissue engineering applications, *Acta Biomater.* 6 (2010) 418–428, <https://doi.org/10.1016/j.actbio.2009.07.012>.
- [21] D.M. García Cruz, J.L. Gomez Ribelles, M. Salmerón Sánchez, Blending polysaccharides with biodegradable polymers. I. Properties of chitosan/poly-caprolactone blends, *J. Biomed. Mater. Res. B Appl. Biomater.* 85 (2008) 303–313, <https://doi.org/10.1002/jbm.b.30947>.
- [22] F. Du, H. Wang, W. Zhao, D. Li, D. Kong, J. Yang, Y. Zhang, Gradient nanofibrous chitosan/poly ε-caprolactone scaffolds as extracellular microenvironments for vascular tissue engineering, *Biomaterials* 33 (2012) 762–770, <https://doi.org/10.1016/j.biomaterials.2011.10.037>.
- [23] Y. Yao, J. Wang, Y. Cui, R. Xu, Z. Wang, J. Zhang, K. Wang, Y. Li, Q. Zhao, D. Kong, Effect of sustained heparin release from PCL/chitosan hybrid small-diameter vascular grafts on anti-thrombotic property and endothelialization, *Acta Biomater.* 10 (2014) 2739–2749, <https://doi.org/10.1016/j.actbio.2014.02.042>.
- [24] A. Cooper, N. Bhattarai, F.M. Kievit, M. Rossol, M. Zhang, Electrospinning of chitosan derivative nanofibers with structural stability in an aqueous environment, *Phys. Chem. Chem. Phys.* 13 (2011) 9969–9972, <https://doi.org/10.1039/C0CP02909B>.
- [25] T. Honma, T. Senda, Y. Inoue, Thermal properties and crystallization behaviour of blends of poly(ε-caprolactone) with chitin and chitosan, *Polym. Int.* 52 (2003) 1839–1846, <https://doi.org/10.1002/pi.1380>.
- [26] S.D. Vrieze, P. Westbroek, T.V. Camp, L.V. Langenhove, Electrospinning of chitosan nanofibrous structures: feasibility study, *J. Mater. Sci.* 42 (2007) 8029–8034, <https://doi.org/10.1007/s10853-006-1485-6>.
- [27] R. Jayakumar, M. Prabaharan, S.V. Nair, H. Tamura, Novel chitin and chitosan nanofibers in biomedical applications, *Biotechnol. Adv.* 28 (2010) 142–150, <https://doi.org/10.1016/j.biotechadv.2009.11.001>.
- [28] L. Wu, H. Li, S. Li, X. Li, X. Yuan, X. Li, Y. Zhang, Composite fibrous membranes of PLGA and chitosan prepared by electrospinning and coaxial electrospinning, *J. Biomed. Mater. Res. A.* 92 (2010) 563–574, <https://doi.org/10.1002/jbm.a.32393>.
- [29] M. Rahmouni, F. Chouinard, F. Nekka, V. Lenaerts, J.C. Leroux, Enzymatic degradation of cross-linked high amylose starch tablets and its effect on in vitro release of sodium diclofenac, *Eur. J. Pharm. Biopharm.* 51 (2001) 191–198, [https://doi.org/10.1016/S0939-6411\(01\)00127-8](https://doi.org/10.1016/S0939-6411(01)00127-8).
- [30] M. Dufresne, P. Bacchin, G. Cerino, J.C. Remigy, G.N. Adrianus, P. Aimar, C. Legallais, Human hepatic cell behavior on polysulfone membrane with double porosity level, *J. Membr. Sci.* 428 (2013) 454–461, <https://doi.org/10.1016/j.memsci.2012.10.041>.
- [31] T. Honma, L. Zhao, N. Asakawa, Y. Inoue, Poly(ε-Caprolactone)/Chitin and poly(ε-caprolactone)/chitosan blend films with compositional gradients: fabrication and their biodegradability, *Macromol. Biosci.* 6 (2006) 241–249, <https://doi.org/10.1002/mabi.200500216>.
- [32] K.T. Shalumon, K.H. Anulekha, C.M. Girish, R. Prasanth, S.V. Nair, R. Jayakumar, Single step electrospinning of chitosan/poly(caprolactone) nanofibers using formic acid/acetone solvent mixture, *Carbohydr. Polym.* 80 (2010) 413–419, <https://doi.org/10.1016/j.carbpol.2009.11.039>.
- [33] I. Olabarrieta, D. Forsström, U.W. Gedde, M.S. Hedenqvist, Transport properties of chitosan and when blended with poly(ε-caprolactone) assessed by standard permeability measurements and microcalorimetry, *Polymer* 42 (2001) 4401–4408, [https://doi.org/10.1016/S0032-3861\(00\)00680-7](https://doi.org/10.1016/S0032-3861(00)00680-7).
- [34] A. Sarasam, S.V. Madhally, Characterization of chitosan-polycaprolactone blends for tissue engineering applications, *Biomaterials* 26 (2005) 5500–5508, <https://doi.org/10.1016/j.biomaterials.2005.01.071>.
- [35] A.R. Sarasam, P. Brown, S.S. Khajotia, J.J. Dmytryk, S.V. Madhally, Antibacterial activity of chitosan-based matrices on oral pathogens, *J. Mater. Sci. Mater. Med.* 19 (2008) 1083–1090, <https://doi.org/10.1007/s10856-007-3072-z>.
- [36] A.R. Sarasam, R.K. Krishnaswamy, S.V. Madhally, Blending chitosan with Polycaprolactone: effects on physicochemical and antibacterial properties, *Biomacromolecules* 7 (2006) 1131–1138, <https://doi.org/10.1021/bm050935d>.
- [37] A.R. Sarasam, A.I. Samli, L. Hess, M.A. Ihnat, S.V. Madhally, Blending chitosan with polycaprolactone: porous scaffolds and toxicity, *Macromol. Biosci.* 7 (2007) 1160–1167, <https://doi.org/10.1002/mabi.200700001>.
- [38] H. She, X. Xiao, R. Liu, Preparation and characterization of polycaprolactone-chitosan composites for tissue engineering applications, *J. Mater. Sci.* 42 (2007) 8113–8119, <https://doi.org/10.1007/s10853-007-1706-7>.
- [39] L. Van der Schueren, B. De Schoenmaker, Ö.I. Kalaoglu, K. De Clerck, An alternative solvent system for the steady state electrospinning of polycaprolactone, *Eur. Polym. J.* 47 (2011) 1256–1263, <https://doi.org/10.1016/j.eurpolymj.2011.02.025>.
- [40] L. Van der Schueren, I. Steyaert, B. De Schoenmaker, K. De Clerck, Polycaprolactone/chitosan blend nanofibres electrospun from an acetic acid/formic acid solvent system, *Carbohydr. Polym.* 88 (2012) 1221–1226, <https://doi.org/10.1016/j.carbpol.2012.01.085>.
- [41] H. Strathmann, K. Kock, P. Amar, R.W. Baker, The formation mechanism of asymmetric membranes, *Desalination* 16 (1975) 179–203, [https://doi.org/10.1016/S0011-9164\(00\)82092-5](https://doi.org/10.1016/S0011-9164(00)82092-5).
- [42] W.S. Rasband, ImageJ, U. S. National Institutes of Health, Bethesda, Maryland,



- USA, 1997, <https://imagej.nih.gov/ij/>.
- [43] L. Benavente, C. Coetsier, A. Venault, Y. Chang, C. Causserand, P. Bacchin, P. Aimar, FTIR mapping as a simple and powerful approach to study membrane coating and fouling, *J. Membr. Sci.* 520 (12) (2016) 477–489, <https://doi.org/10.1016/j.memsci.2016.07.061>.
- [44] P. Das, S. Salerno, J.-C. Remigy, J.-F. Lahitte, P. Bacchin, L. De Bartolo, Double porous poly( $\epsilon$ -caprolactone)/chitosan membrane scaffolds as niches for HUMAN Mesenchymal Stem Cells, *Colloids Surfaces B Biointerfaces* 184 (2019), <https://doi.org/10.1016/j.colsurfb.2019.110493> 110493.
- [45] P. Das, A.D. van der Meer, A. Vivas, Y.B. Arik, J.-C. Remigy, J.-F. Lahitte, R.G.H. Lammertink, P. Bacchin, Tunable microstructured membranes in organs-on-chips to monitor transendothelial hydraulic resistance, *Tissue Eng. A* (2019), <https://doi.org/10.1089/ten.tea.2019.0021>.
- [46] M.N.V.R. Kumar, R.A.A. Muzzarelli, C. Muzzarelli, H. Sashiwa, A.J. Domb, Chitosan chemistry and pharmaceutical perspectives, *Chem. Rev.* 104 (2004) 6017–6084, <https://doi.org/10.1021/cr030441b>.
- [47] P.J. Flory, *Principles of Polymer Chemistry*, Cornell University Press, Ithaca, NY, 1953.
- [48] C. Vogel, E. Wessel, H.W. Siesler, FT-IR imaging spectroscopy of phase separation in blends of poly(3-hydroxybutyrate) with poly(L-lactic acid) and poly( $\epsilon$ -caprolactone), *Biomacromolecules* 9 (2008) 523–527, <https://doi.org/10.1021/bm701035p>.
- [49] Y. Wan, X. Lu, S. Dalai, J. Zhang, Thermophysical properties of polycaprolactone/chitosan blend membranes, *Thermochim. Acta* 487 (2009) 33–38, <https://doi.org/10.1016/j.tca.2009.01.007>.
- [50] H. Zhang, X. Luo, X. Lin, X. Lu, Y. Zhou, Y. Tang, Polycaprolactone/chitosan blends: simulation and experimental design, *Mater. Des.* 90 (2016) 396–402, <https://doi.org/10.1016/j.matdes.2015.10.108>.
- [51] M. Borjigin, C. Eskridge, R. Niamat, B. Strouse, P. Bialk, E.B. Kmiec, Electrospun fiber membranes enable proliferation of genetically modified cells, *Int. J. Nanomed.* 8 (2013) 855–864, <https://doi.org/10.2147/IJN.S40117>.
- [52] V.M. Correlo, L.F. Boesel, M. Bhattacharya, J.F. Mano, N.M. Neves, R.L. Reis, Properties of melt processed chitosan and aliphatic polyester blends, *Mater. Sci. Eng. A* 403 (2005) 57–68, <https://doi.org/10.1016/j.msea.2005.04.055>.
- [53] N. Niamsa, A. Puntumchai, Y. Sutthikhum, Y. Srisuwan, Y. Baimark, Preparation and characterization of biodegradable chitosan and methoxy poly(ethylene glycol)-b-poly( $\epsilon$ -caprolactone) blend homogeneous films, *J. Appl. Polym. Sci.* 109 (2008) 418–423, <https://doi.org/10.1002/app.28117>.
- [54] Y. Chatani, Y. Okita, H. Tadokoro, Y. Yamashita, Structural studies of polyesters. III. Crystal structure of poly- $\epsilon$ -caprolactone, *Polym. J.* 1 (1970) 555, <https://doi.org/10.1295/polymj.1.555>.
- [55] S. Ramakrishna, K. Fujihara, W.E. Teo, T.C. Lim, Z. Ma, *An Introduction to Electrospinning and Nanofibers*, Ed. *World Scientific*, 2005.
- [56] F.S. Kittur, K.V. Harish Prashanth, K. Udaya Sankar, R.N. Tharanathan, Characterization of chitin, chitosan and their carboxymethyl derivatives by differential scanning calorimetry, *Carbohydr. Polym.* 49 (2002) 185–193, [https://doi.org/10.1016/S0144-8617\(01\)00320-4](https://doi.org/10.1016/S0144-8617(01)00320-4).
- [57] M. Mucha, A. Pawlak, Thermal analysis of chitosan and its blends, *Thermochim. Acta* 427 (2005) 69–76, <https://doi.org/10.1016/j.tca.2004.08.014>.
- [58] T. Nishi, T.T. Wang, Melting point depression and kinetic effects of cooling on crystallization in poly(vinylidene fluoride)-Poly(methyl methacrylate) mixtures, *Macromolecules* 8 (1975) 909–915, <https://doi.org/10.1021/ma60048a040>.
- [59] H.S. Azevedo, F.M. Gama, R.L. Reis, In vitro assessment of the enzymatic degradation of several starch based biomaterials, *Biomacromolecules* 4 (2003) 1703–1712, <https://doi.org/10.1021/bm0300397>.
- [60] H.S. Azevedo, R.L. Reis, Understanding the enzymatic degradation of biodegradable polymers and strategies to control their degradation rate, *Biodegrad. Syst. Tissue Eng. Regen. Med.* (2005) 177–201, <https://doi.org/10.1201/9780203491232.ch12>.
- [61] J.S. Chawla, M.M. Amiji, Biodegradable poly( $\epsilon$ -caprolactone) nanoparticles for tumor-targeted delivery of tamoxifen, *Int. J. Pharm.* 249 (2002) 127–138, [https://doi.org/10.1016/S0378-5173\(02\)00483-0](https://doi.org/10.1016/S0378-5173(02)00483-0).
- [62] A.M. Martins, Q.P. Pham, P.B. Malafaya, R.A. Sousa, M.E. Gomes, R.M. Raphael, F.K. Kasper, R.L. Reis, A.G. Mikos, The role of lipase and alpha-amylase in the degradation of starch/poly(epsilon-caprolactone) fiber meshes and the osteogenic differentiation of cultured marrow stromal cells, *Tissue Eng. A* 15 (2009) 295–305, <https://doi.org/10.1089/ten.tea.2008.0025>.
- [63] K. Tomihata, Y. Ikada, In vitro and in vivo degradation of films of chitin and its deacetylated derivatives, *Biomaterials* 18 (1997) 567–575, [https://doi.org/10.1016/S0142-9612\(96\)00167-6](https://doi.org/10.1016/S0142-9612(96)00167-6).
- [64] K.M. Vårnum, M.M. Myhr, R.J.N. Hjerde, O. Smidsrød, In vitro degradation rates of partially N-acetylated chitosans in human serum, *Carbohydr. Res.* 299 (1997) 99–101, [https://doi.org/10.1016/S0008-6215\(96\)00332-1](https://doi.org/10.1016/S0008-6215(96)00332-1).
- [65] H. Sashiwa, H. Saimoto, Y. Shigemasa, R. Ogawa, S. Tokura, Lysozyme susceptibility of partially deacetylated chitin, *Int. J. Biol. Macromol.* 12 (1990) 295–296, [https://doi.org/10.1016/0141-8130\(90\)90016-4](https://doi.org/10.1016/0141-8130(90)90016-4).
- [66] S. Hirano, H. Tsuchida, N. Nagao, N-acetylation in chitosan and the rate of its enzymic hydrolysis, *Biomaterials* 10 (1989) 574–576, [https://doi.org/10.1016/0142-9612\(89\)90066-5](https://doi.org/10.1016/0142-9612(89)90066-5).
- [67] X. Zhong, C. Ji, A.K.L. Chan, S.G. Kazarian, A. Ruys, F. Dehghani, Fabrication of chitosan/poly( $\epsilon$ -caprolactone) composite hydrogels for tissue engineering applications, *J. Mater. Sci. Mater. Med.* 22 (2011) 279–288, <https://doi.org/10.1007/s10856-010-4194-2>.
- [68] R. Mad Jin, N. Sultana, S. Baba, S. Hamdan, A.F. Ismail, Porous PCL/chitosan and nHA/PCL/chitosan scaffolds for tissue engineering applications: fabrication and evaluation, *J. Nanomater.* (2015), <https://doi.org/10.1155/2015/357372>.
- [69] C. Hansen, *Hansen Solubility Parameters: A User's Handbook*, Second, CRC Press, Boca Raton, Fla, 2007, <https://www.hansen-solubility.com/>, Accessed date: 16 March 2018.
- [70] R. Ravindra, K.R. Krovvidi, A.A. Khan, Solubility parameter of chitin and chitosan, *Carbohydr. Polym.* 36 (1998) 121–127, [https://doi.org/10.1016/S0144-8617\(98\)00020-4](https://doi.org/10.1016/S0144-8617(98)00020-4).
- [71] R.J. Lehnert, A. Kandelbauer, Comments on “solubility parameter of chitin and chitosan” carbohydrate polymers 36 (1998) 121–127, *Carbohydr. Polym.* 175 (2017) 601–602, <https://doi.org/10.1016/j.carbpol.2017.07.079>.
- [72] C. Bordes, V. Fréville, E. Ruffin, P. Marote, J.Y. Gauvrit, S. Briançon, P. Lantéri, Determination of poly( $\epsilon$ -caprolactone) solubility parameters: application to solvent substitution in a microencapsulation process, *Int. J. Pharm.* 383 (2010) 236–243, <https://doi.org/10.1016/j.ijpharm.2009.09.023>.
- [73] C.N. Costa, V.G. Teixeira, M.C. Delpech, J.V.S. Souza, M.A.S. Costa, Viscometric study of chitosan solutions in acetic acid/sodium acetate and acetic acid/sodium chloride, *Carbohydr. Polym.* 133 (2015) 245–250, <https://doi.org/10.1016/j.carbpol.2015.06.094>.
- [74] H. Strathmann, K. Kock, The formation mechanism of phase inversion membranes, *Desalination* 21 (1977) 241–255, [https://doi.org/10.1016/S0011-9164\(00\)88244-2](https://doi.org/10.1016/S0011-9164(00)88244-2).
- [75] G.R. Guillen, Y. Pan, M. Li, E.M.V. Hoek, Preparation and characterization of membranes formed by nonsolvent induced phase separation: a review, *Ind. Eng. Chem. Res.* 50 (2011) 3798–3817, <https://doi.org/10.1021/ie101928r>.
- [76] J.C. Remigy, M. Meireles, X. Thibault, Morphological characterization of a polymeric microfiltration membrane by synchrotron radiation computed microtomography, *J. Membr. Sci.* 305 (2007) 27–35, <https://doi.org/10.1016/j.memsci.2007.06.059>.
- [77] P. Das, J.-F. Lahitte, J.-C. Remigy, B. Garmy-Susini, S. Desclaux, C. Coetsier, L. De Bartolo, P. Bacchin, Artificial membranes tuning for lymphatic wall repair, *Eur. Chapter Meet. Tissue Eng. Regen. Med. Int. Soc. TERMIS-EU 2016*, Uppsala, Sweden, 2016, p. 101 <https://hal.archives-ouvertes.fr/hal-01360666>, Accessed date: 13 December 2017.
- [78] S.M. Casillo, A.P. Peredo, S.J. Perry, H.H. Chung, T.R. Gaborski, Membrane pore spacing can modulate endothelial cell-substrate and cell-cell interactions, *ACS Biomater. Sci. Eng.* 3 (2017) 243–248, <https://doi.org/10.1021/acsbiomaterials.7b00055>.
- [79] S.H. Ranganath, O. Levy, M.S. Inamdar, J.M. Karp, Harnessing the mesenchymal stem cell secretome for the treatment of cardiovascular disease, *Cell Stem Cell* 10 (2012) 244–258, <https://doi.org/10.1016/j.stem.2012.02.005>.
- [80] F.A. Fierro, N. Magner, J. Beegle, H. Dahlenburg, J.L. White, P. Zhou, K. Pepper, B. Fury, D.P. Coleal-Bergum, G. Bauer, W. Gruenloh, G. Annett, C. Pifer, J.A. Nolte, Mesenchymal stem/stromal cells genetically engineered to produce vascular endothelial growth factor for revascularization in wound healing and ischemic conditions, *Transfusion (Paris)* 59 (2019) 893–897, <https://doi.org/10.1111/trf.14914>.
- [81] F. Yang, S.-W. Cho, S.M. Son, S.R. Bogatyrev, D. Singh, J.J. Green, Y. Mei, S. Park, S.H. Bhang, B.-S. Kim, R. Langer, D.G. Anderson, Genetic engineering of human stem cells for enhanced angiogenesis using biodegradable polymeric nanoparticles, *Proc. Natl. Acad. Sci.* 107 (2010) 3317–3322, <https://doi.org/10.1073/pnas.0905432106>.
- [82] F.A.L.M. Eskens, J. Verweij, The clinical toxicity profile of vascular endothelial growth factor (VEGF) and vascular endothelial growth factor receptor (VEGFR) targeting angiogenesis inhibitors: A review, *Eur. J. Cancer* 42 (2006) 3127–3139, <https://doi.org/10.1016/j.ejca.2006.09.015>.
- [83] A. Di Luca, B. Ostrowska, I. Lorenzo-Moldero, A. Lepedda, W. Swieszkowski, C. Van Blitterswijk, L. Moroni, Gradients in pore size enhance the osteogenic differentiation of human mesenchymal stromal cells in three-dimensional scaffolds, *Sci. Rep.* 6 (2016), <https://doi.org/10.1038/srep22898>.
- [84] P. Kasten, I. Beyen, P. Niemeyer, R. Luginbühl, M. Bohner, W. Richter, Porosity and pore size of  $\beta$ -tricalcium phosphate scaffold can influence protein production and osteogenic differentiation of human mesenchymal stem cells: an in vitro and in vivo study, *Acta Biomater.* 4 (2008) 1904–1915, <https://doi.org/10.1016/j.actbio.2008.05.017>.
- [85] R. Kramann, C. Goettsch, J. Wongboonsin, H. Iwata, R.K. Schneider, C. Kuppe, N. Kaesler, M. Chang-Panesso, F.G. Machado, S. Gratwohl, K. Madhurima, J.D. Hutcheson, S. Jain, E. Aikawa, B.D. Humphreys, Adventitial MSC-like cells are progenitors of vascular smooth muscle cells and drive vascular calcification in chronic kidney disease, *Cell Stem Cell* 19 (2016) 628–642, <https://doi.org/10.1016/j.stem.2016.08.001>.
- [86] X. Zhang, M.P. Bendeck, C.A. Simmons, J.P. Santerre, Deriving vascular smooth muscle cells from mesenchymal stromal cells: evolving differentiation strategies and current understanding of their mechanisms, *Biomaterials* 145 (2017) 9–22, <https://doi.org/10.1016/j.biomaterials.2017.08.028>.
- [87] M. Floren, W. Bonani, A. Dharmarajan, A. Motta, C. Migliaresi, W. Tan, Human mesenchymal stem cells cultured on silk hydrogels with variable stiffness and growth factor differentiate into mature smooth muscle cell phenotype, *Acta Biomater.* 31 (2016) 156–166, <https://doi.org/10.1016/j.actbio.2015.11.051>.